Chapter 33 – SEMI-EMPIRICAL PREDICTION OF VORTEX ONSET ON THE VFE-2 CONFIGURATION

by

Raj K. Nangia

ABSTRACT

This paper, via the initiative of the RTO-AVT Task Group AVT-113, is concerned with the VFE-2 theoretical and experimental activities on a series of 65° delta wings with different leading edge bluntness (sharp, small, medium and large radius). Experimental results have included independent sweeps of Mach and Reynolds number in the NTF wind tunnel.

Onset of vortical flow is predicted on the basis of semi-empirical attained leading edge thrust considerations. The approach based originally on Carlson's work at NASA, also incorporates centre section and wing tip modifications of the sheared wing concept according to Kuchemann.

Flow is assumed to be attached in regions with predicted LE suctions below the criteria developed from 2-D suction limits. Where the predicted LE suctions are above the criteria, the flow is assumed to be separated and this allows the determination of onset of vortical flow that is handled, using Polhamus LE suction analogy.

The method has been applied to all VFE-2 configurations. Results are compared with experimental data from NASA and ONERA Tests. Good agreement has been obtained for small and medium radius LE.

The vortex onset information together with a knowledge of forces, moments and loadings provides an understanding for either exploitation or avoidance in the wider design perspective. This is an important motivation.

33.1 NOMENCLATURE

AR or A	Aspect Ratio
B = 2 s	Wing span
c	Local Wing Chord (streamwise x direction)
$c_{av} = c_{ref} = S/b$	Mean Geometric Chord
$\bar{c} = c_{bar}$	Mean Aerodynamic Chord
c_n	Normal chord, effective, see Figure 33-23
c_r	Root chord
c_t	Tip chord (0 for deltas)
C_A = Axial force/(q S)	Axial Force Coefficient
C_{AL}	Local Axial Force Coefficient
C_D or C_{Di}	Lift-induced Drag Force/(q S), Lift-induced Drag Coefficient
C_{DL}	Local Lift-induced Drag Coefficient

CG	Centre of Gravity
C_L = Lift Force/(q S)	Lift Coefficient
C_{LL}	Local Lift Coefficient
C_{TL}	Local Thrust Coefficient, normal to LE
C_p	Coefficient of Pressure
C_{pcrit}	Sonic C_p
C_{plim}	Limiting C_p
C_{pvac}	Vacuum limit on C_p
c_t = LE	Thrust in chordwise direction, in certain figures due to Carlson, e.g. Figure 33-13
$c_{t,n} = C_{TL}$	Coefficient of LE Thrust, normal to LE
dt	Parameter for delay in onset of flow separation due to thickness
$k = \pi A\ C_{Di} / C_L^2$	Lift Induced Drag Factor
$K_T = C_{plim}/C_{pvac}$	Thrust Factor
LE, TE	Leading Edge, Trailing Edge
M	Mach Number
M_n	Mach Number normal to LE
$q = 0.5\ \rho\ V^2$	Dynamic Pressure, ρ Air Density
$r = r_{le}$	LE radius in streamwise direction
r_n	LE radius normal to LE
Re	Reynolds Number, based on c_{av}
$R_n = R_{mac}$	Reynolds Number, based on mean aerodynamic chord as used by Luckring, 6 million and 60 million
R_n	Reynolds Number, based on c_n (chord normal to LE), used only in Sections 33.3.2 and 33.3.3, and Figure 33-16 – Figure 33-23
s, S	Semi-span, Wing Area respectively
t	Local maximum thickness along chord
t_n	Local maximum thickness in direction, normal to LE
t/c	Local thickness/chord ratio at a spanwise station
x,y,z	Orthogonal co-ordinates
x_m	Position of maximum thickness along chord
x_v,y_v	Position of vortex onset
V	Free-stream Velocity
α	AoA, Alpha, Angle of Attack
α_{BD}	AoA, Alpha, Angle of Attack for Vortex Breakdown onset at Trailing Edge
ß	Sideslip angle
γ	Ratio of specific heat constants for flow medium, γ = 1.4 for air
Λ	LE Sweep Angle
η = y/s	Non-dimensional spanwise distance

33.2 INTRODUCTION AND BACKGROUND

For highly manoeuvrable or advanced aircraft, manned / unmanned, it is imperative to understand the onset of wing vortex flows and their breakdown and the prospects of controlling them [33-1]. The applications are to military and civil type wings featuring moderate to high sweep.

An understanding of vortex flows in symmetric and asymmetric flow is required from the viewpoint of control and also, for example, the design of LE / TE devices**.** We need qualitative and quantitative information on vortex flows, e.g. forces, moments and loadings so as to either exploit them or avoid them, e.g. by using camber and twist. This design perspective is an important motivation from our viewpoint.

The challenge seen here is to predict forces and moments on a wing-body (deltas and swept tapered wings, cambered, rounded LE) operating in symmetric or asymmetric conditions throughout a full α range with Mach and Reynolds number effects. Furthermore, a quick turn-around is needed to cope with many geometric and flow variables.

The RTO-AVT has been interested in vortex flows and a recent task group, involving several countries and researchers, was the AVT-080 [33-2]. Our part of the work for that group was reported for wider circulation in Refs. [33-2], [33-3].

This Paper is motivated via the initiative of the RTO-AVT Task group AVT-113. One of the tasks (VFE-2) is concerned with theoretical and experimental activities on a series of 65° delta wings with differing LE bluntness, initiated by Luckring at NASA LaRC [33-4]-[33-6].

The NASA delta wing (Figure 33-1) with one sharp and three rounded leading edge geometries (Figure 33-2) has been tested at the NASA Langley NTF facility (Figure 33-3) at various Mach and Reynolds number combinations. Recently the model was tested in the DNW Transonic Wind Tunnel (TWG) at DLR Goettingen, in the low speed facilities at ONERA Lille and also in the Turkish facilities at Ankara. The model has non-standard aerofoil sections. Figure 33-4 shows the effective semi-span t/c and r/c distributions.

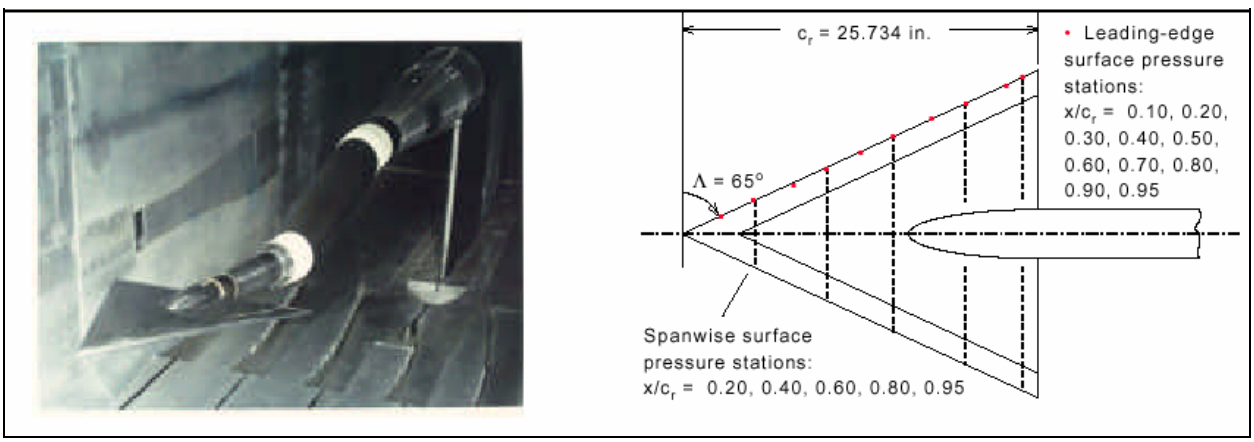

(a) Model Installed in NTF **(b) Instrumentation Layout**

Figure 33-1: NTF 65° Delta Wing (Luckring).

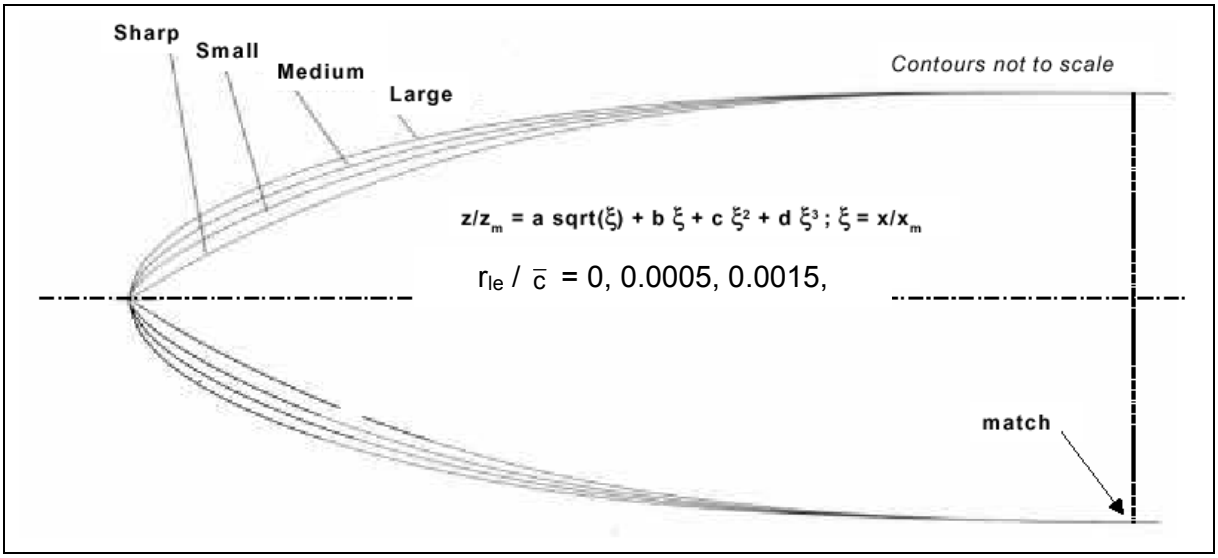

Figure 33-2: Streamwise Leading-Edge Contours for NTF Delta Wings (Luckring).

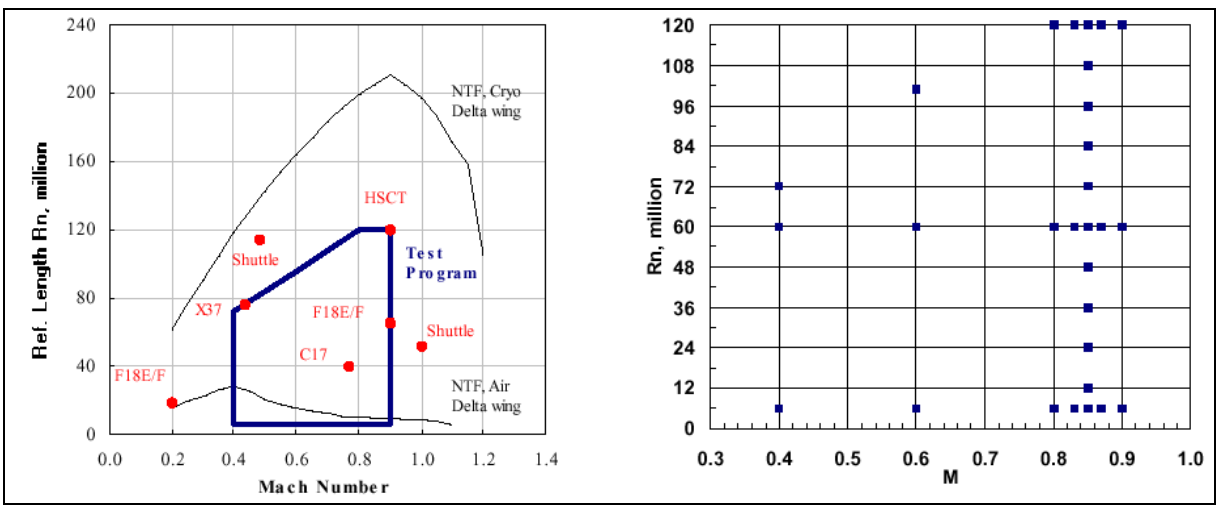

(a) NTF Envelopes and Aircraft Operation **(b) Representative Delta-Wing Test Matrix**

Figure 33-3: Reynolds Number and Mach Number Conditions (NASA LaRC, Luckring).

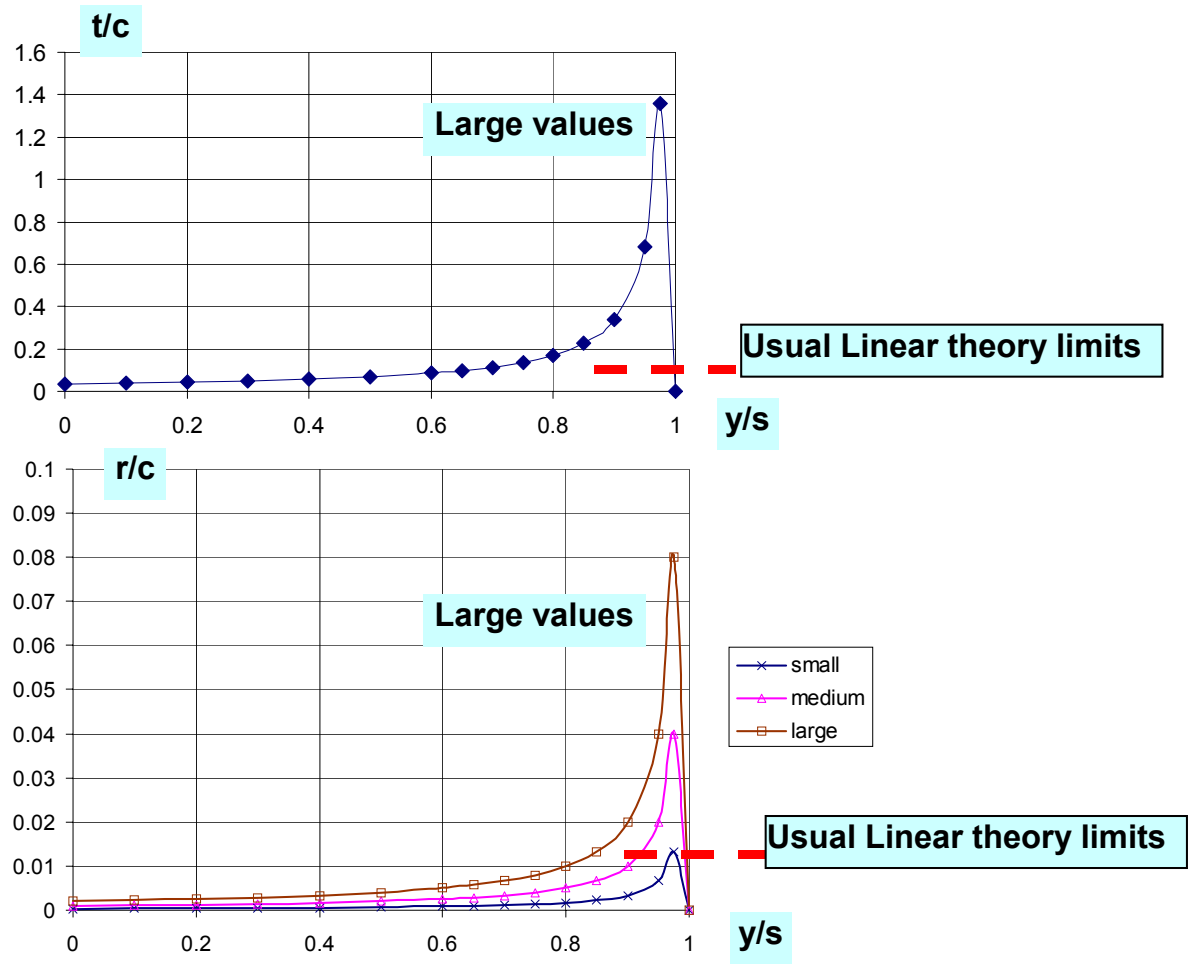

Figure 33-4: Delta Wing, t/c and r/c Variations with y/s for Rounded Edge Models.

From the NASA results (Luckring, Refs. [33-4]-[33-6], all wings), Figure 33-5-Figure 33-8 depict the position of onset of vortical flow, x_v measured from the wing apex, as a function of angle of attack (AoA or α), Mach number and Reynolds number (2 settings, R_{mac} = 6 million & 60 million, based on mean aerodynamic chord). The model geometries and results are reviewed and discussed in more detail in Section 33.4.

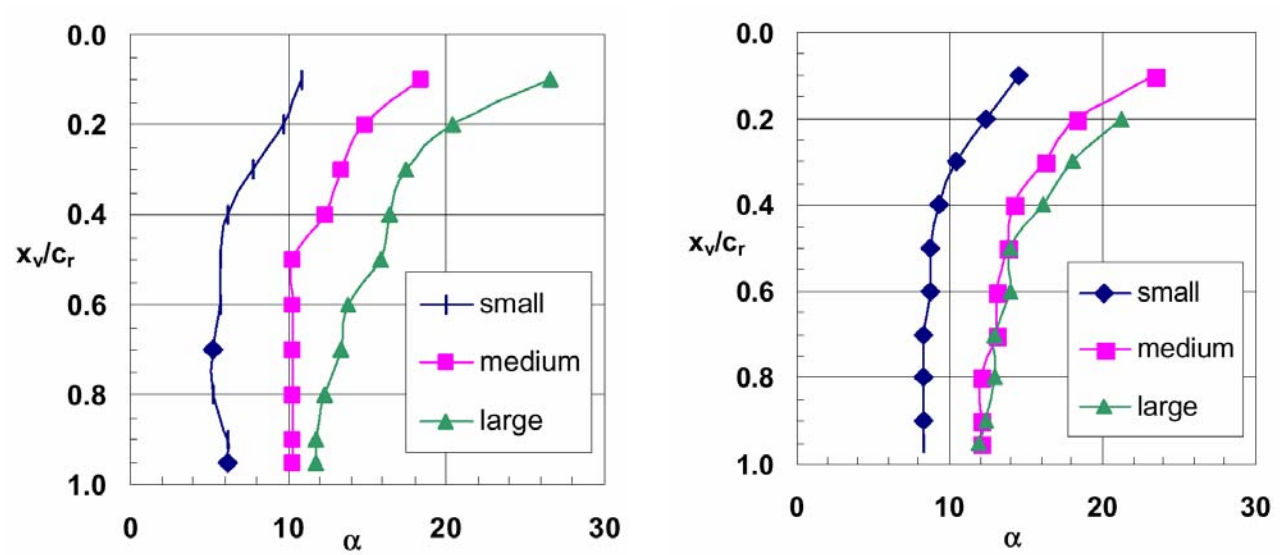

R_{mac} = 6 million

R_{mac} = 60 million

Figure 33-5: Models with Small, Medium and Large Roundness, Flow Separation (LE Vortex) Onset and Movement, Effect of R_{mac}, Mach 0.4.

AIAA-2004-0765

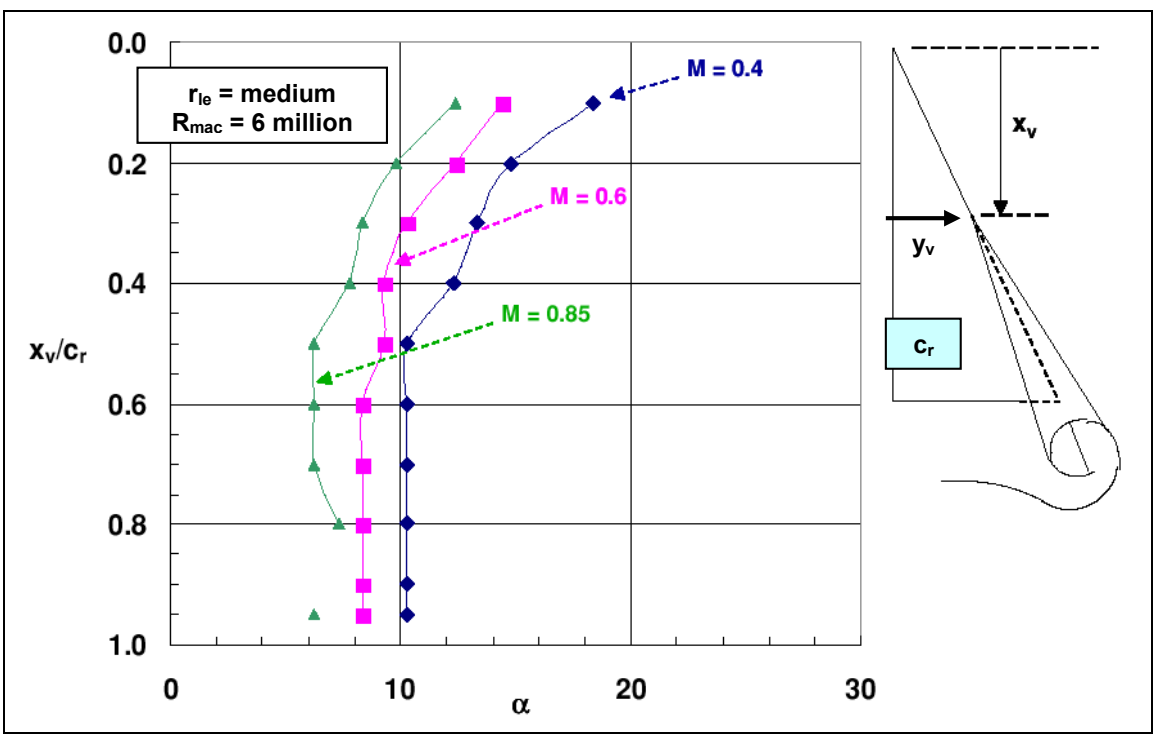

Figure 33-6: Model with Medium Round LE, Flow Separation Onset and Movement, Effect of Compressibility, Mach 0.4, 0.6 & 0.85, R_{mac} = 6 Million.

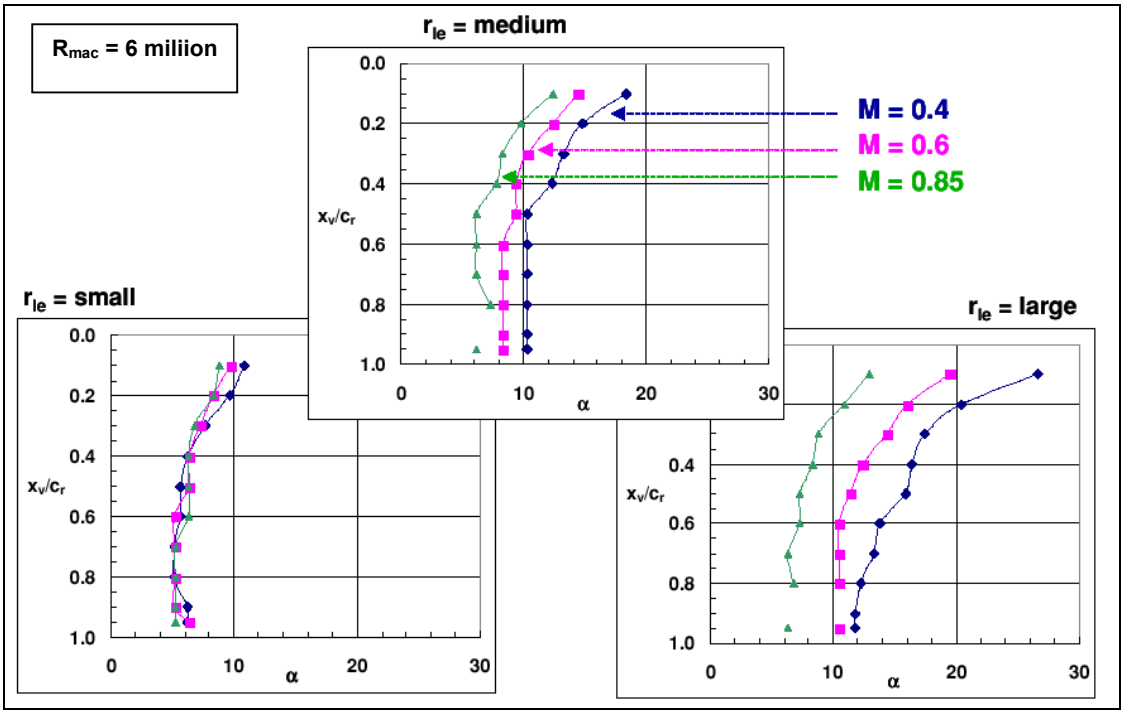

Figure 33-7: Models with Small, Medium and Large Roundness LE, Flow Separation Onset and Movement, Effect of Compressibility, Mach 0.4, 0.6 & 0.85, R_{mac} = 6 Million.

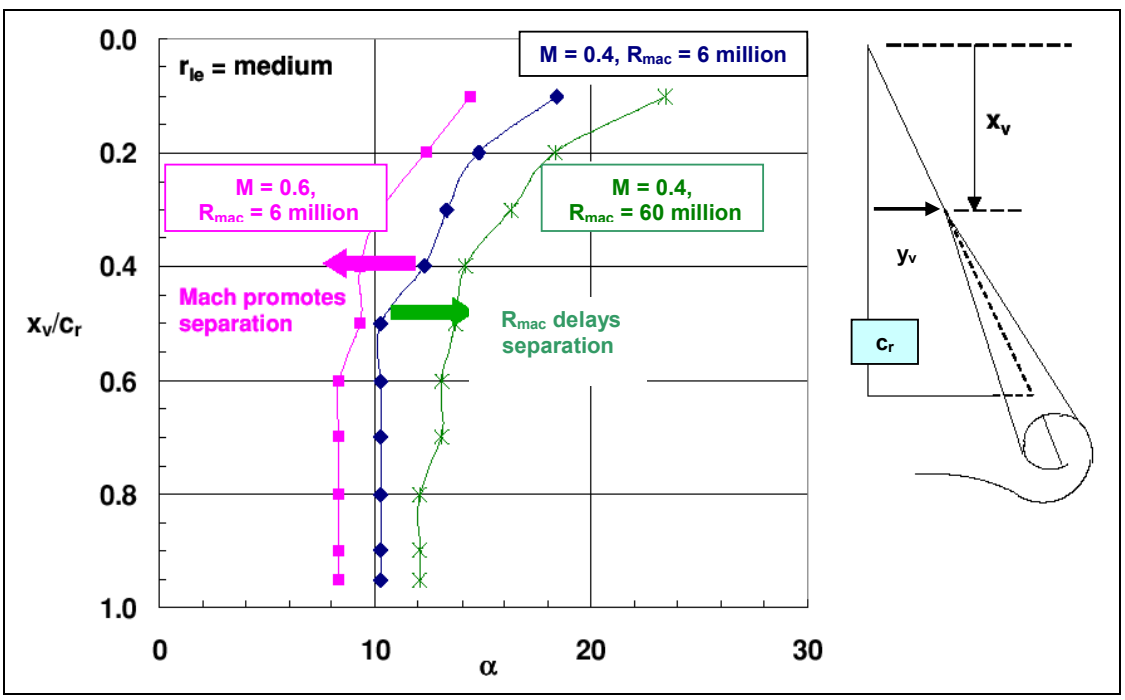

Figure 33-8: Model with Medium LE, Flow Separation Onset and Movement, Effect of Compressibility and R, Mach 0.4 & 0.6, R_{mac} = 6 Million & 60 Million.

Towards a first order perspective at low speeds, it is interesting to reflect on Figure 33-9 from Ref. [33-2] (developed from Refs. [33-7]-[33-8]) to give an idea of the vortex flows domains. It would appear that vortex breakdown would begin to occur at the TE at about 17.5° AoA, at least for sharp LE. At higher Mach numbers, this will occur at lower AoA.

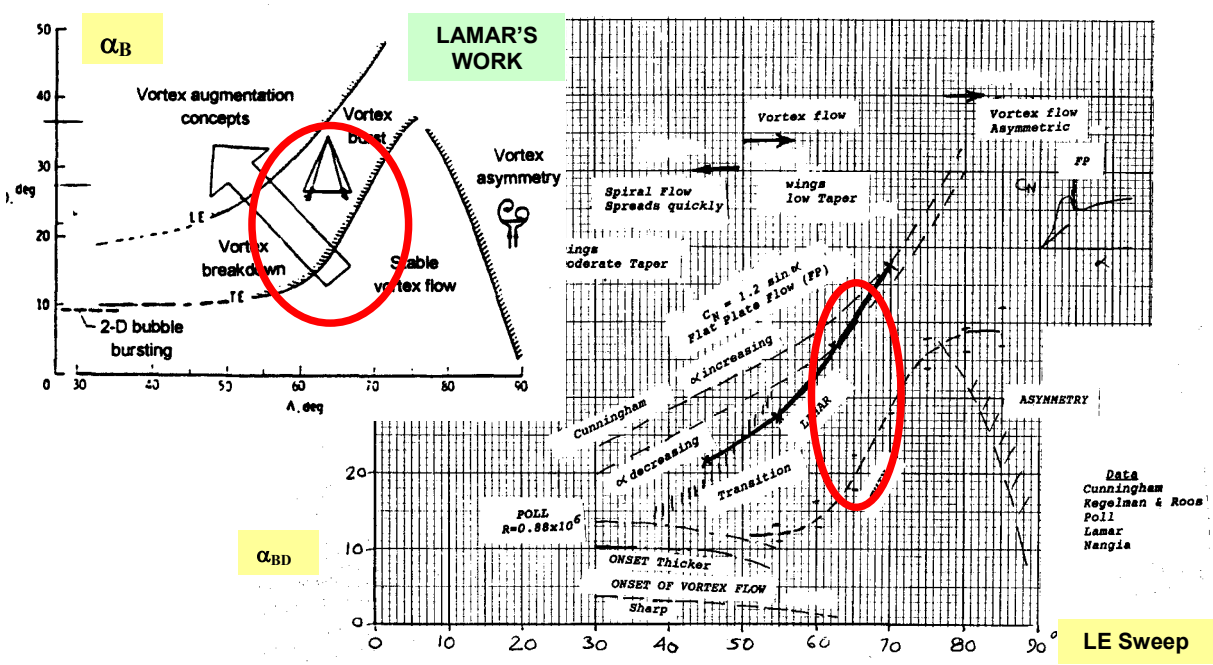

Figure 33-9: Extended Qualification of Vortex Flow Onset, Breakdown and Control, Starting from Lamar's Work.

The onset of the vortical flow will be predicted in this document, using the semi-empirical approach developed by Nangia from the publications of Carlson, Kuchemann, Polhamus and others [33-9]-[33-16].

33.3 PREDICTION APPROACH

We have developed, since the 80's, a theoretical approach based typically on Refs. [33-9]-[33-10]. The method uses an inviscid, subsonic lifting surface theory coupled with semi-empirical "attained" thrust and vortex effects depending upon Mach, Reynolds number and aerofoil geometry (based initially on NASA LaRC work, Carlson and others (Refs. [33-11]-[33-16]) and further developed by Nangia. The method is capable of tackling symmetric and asymmetric flows. Confidence in the basic method has been built up over the years in analysis and design modes (e.g. Refs. [33-17]-[33-18]).

For a given Mach number and wing geometry, the inviscid theory (surface-singularity (panel) method or a thin lifting surface / vortex lattice, or even an Euler) produces the idealized (attached) flow loads, moments and C_p distribution over the whole wing. To a first order, within the limitations of the inviscid approach assumptions, the forces and moments correspond to the "infinite" Reynolds number case. In general, the LE thrust predicted by such codes correlates well with practical situations at low incidences. However, at the higher incidences, the LE thrust attained becomes a reducing proportion of the idealized thrust (flow partly separates). The experience

is also that the thicker wings have wider regions of attached flow, than thinner wings. Sharp LE wings cannot sustain LE suction.

This brings in the need for attained thrust techniques to analyse / predict practical situations with finite Reynolds number effects. The underlying idea is to "scale back" the attained thrust as a function of flow and geometry parameters.

33.3.1 General Approach

With reference to Figure 33-10-Figure 33-11, there are three main features of the attained thrust technique. Essentially the approach works between 2-D and 3-D to predict the forces and moments with attained thrust. The main features are:

a) Prediction of 3-D inviscid aerodynamic characteristics;

b) Evaluation of limits e.g. C_{plim} with Mach and Reynolds number constraints from 2-D considerations;

c) Estimation of the effect of aerofoil parameters; and

d) Using simple sweep theory to connect 2-D and 3-D.

A staged process can be highlighted in the following steps:

1) Define the geometry of the wing. In the present work this is a simple delta planform of root chord c_r. The tip chord c_t is zero. Estimate the aerofoil LE geometry variations on the wing as a function of spanwise co-ordinate y/s. We need LE radius/chord ratio (r/c), thickness/chord ratio (t/c) and position of Maximum thickness along chord (x_m/c).

2) At the given freestream Mach number M, apply an inviscid solver e.g. lifting surface / vortex lattice approach to predict the attached flow aerodynamic characteristics including chordwise loadings and spanwise loadings of Normal and Axial forces (C_{NL} & C_{AL}). For a planar wing, the scaling with AoA effects is simple: C_{NL} increases directly with AoA and C_{AL} is function of AoA squared. From the C_{AL} loadings, we can determine LE suction C_{TL} (c_t , Carlson) along the wing LE. The lift and drag (C_{LL} and C_{DL}) loadings can be obtained with appropriate resolution of the normal and axial loadings.

3) The linear theory attached flow results in Step 2, essentially correspond to 100% LE suction. For wings of "sufficient" LE sweep, we can derive 0% LE suction results simply by using the Polhamus LE suction analogy i.e. turning the LE suction upwards by 90° to give a non-linear vortex lift (combining 2-D & 3-D geometry). The results for 0% LE suction, including the non-linear lift, correspond to a sharp LE wing. The two solutions for 100% and 0% LE suction essentially form the "tram-lines" for the application of attained thrust solutions for other combinations of LE roundness. The 0% LE suction result implies that vortex appears all along the LE at all AoA (either side of AoA = 0°).

4) For wings with "non-sharp" i.e. rounded LE, the onset of vortical flow is delayed. This delay depends on several parameters including Mach number, Reynolds number and Aerofoil geometry parameters (established in Step 1). The "attained thrust" approach (based initially on NASA LaRC work) is applied, together with an adaptation of the Polhamus analogy to "non-attained" thrust. This is discussed in the next Sections 33.3.2 and 33.3.3.

5) If further analysis towards prediction of vortex breakdown is required, then this step, using Lan's method needs to be included. In this report, however, we do not consider this.

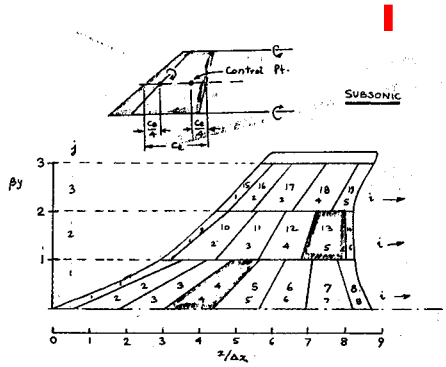

1. Definition of Swept, Cambered Thin Wing Geometry, Aerofoil Geometry

2. At given Mach number, apply an Inviscid Solver Lifting Surface / vortex Lattice Symmetric & Asymmetric situations

3. Determine values for 100% LE Suction Polhamus Analogy for Swept Sharp LE to derive 0% LE suction results "tram lines" Obtained

4. Apply Semi-Empirical "Attained" Thrust Approach, using Mach & Reynolds No. & Aerofoil Geometry Predict Onset of Vortical Flow & Progression

Polhamus Analogy on "non-attained" thrust (sufficiently Swept Edges) Vortex Development

5. Check for Vortex Strength Distribution along Span

If required, apply Lan's Method Vortex Breakdown onset criteria

Figure 33-10: Different Stages in Evaluation Method Incorporating Attained Thrust, LE Suction Analogy and Vortex Breakdown Empiricisms, Symmetric and Asymmetric Situations.

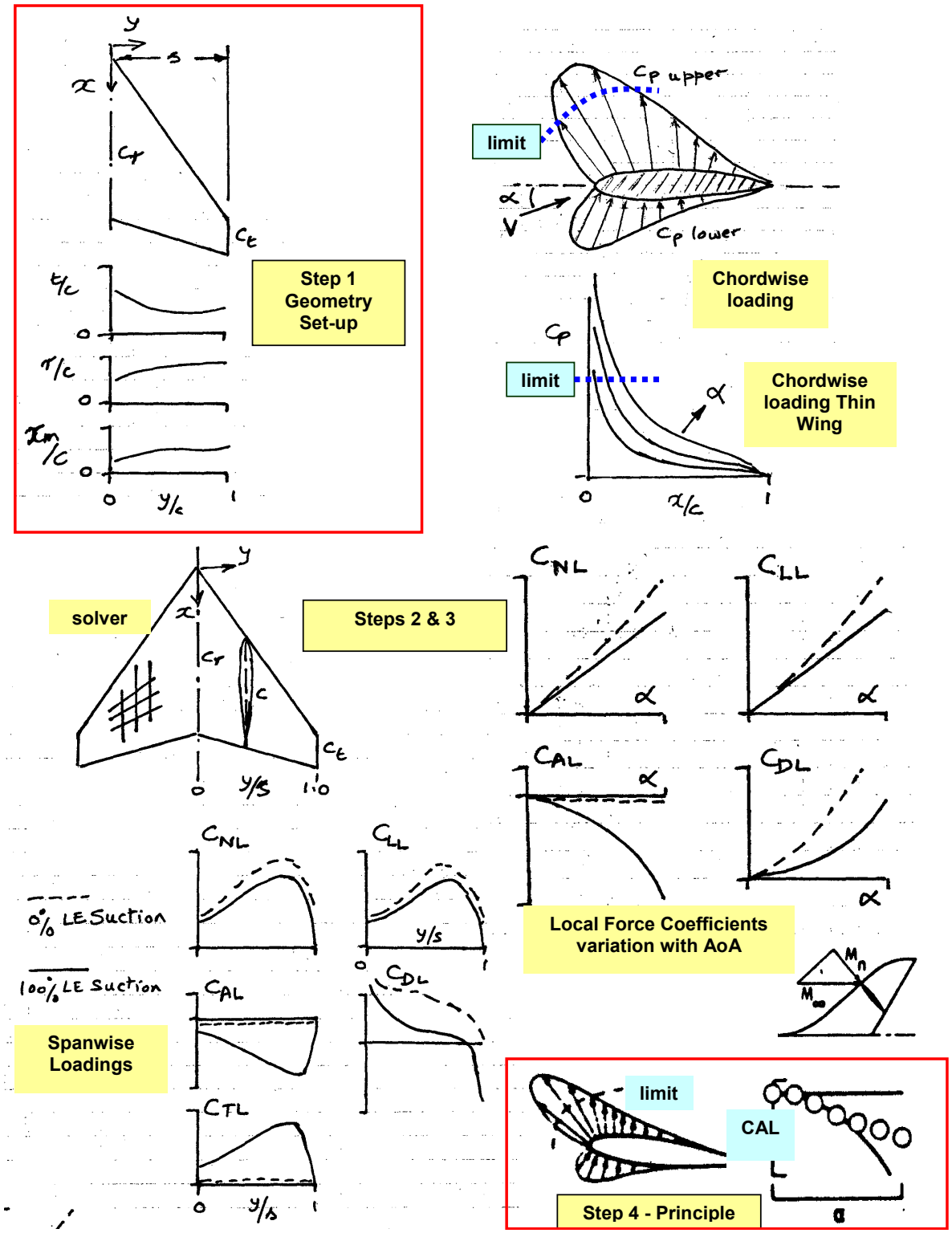

Figure 33-11: Key Features and Various Steps of the Attained Thrust Prediction Method (Carlson et al).

33.3.2 Analysis of Sectional LE Thrust (Based on Carlson's Work)

The inviscid linear lifting surface theory at the given Mach number leads to the description of maximum suction $C_{TL}(y)$ along the LE (Steps 1 – 2 above). In general, at all AoA beyond the LE attachment condition, it is implied that C_p at the LE will be infinite (negative) and the strength of this will vary with AoA. We know that in physical flow this is unrealistic and a limiting value of C_p i.e. C_{plim}, needs to be introduced as sketched in Figure 33-11.

The considerations for C_{plim} are:

- C_p cannot be less than the vacuum limit $C_{pvac} = -2\,\gamma\,/M_n^2$, where M_n is the Mach number normal to the wing LE.
- Effects on $-C_{plim}$ are related to Mach, Reynolds number and the aerofoil parameters. These are conveniently described by curve-fit formulae using C_{pvac} (based on LaRC work and updated by Nangia).

A factor $K_T = C_{plim}/C_{pvac}$ (i.e. relating C_{plim} to C_{pvac}) needs to be determined. The correlations can be built into a prediction method for 3-D wings. At any spanwise station (y/s), the onset of flow separation is predicted when K_T is less than 1.0. Curtailing K_T implies lower magnitudes of C_{TL} and C_{AL} (axial force coefficient).

Figure 33-12 shows the C_{plim} , Mach number and sweep angle Λ relationships. C_{plim} is infinite at M = 0. It is conveniently expressed in terms of the vacuum limit $C_{pvac} = -2\gamma/(M_n^2)$, with $M_n = M\cos\Lambda$. Note that $C_{plim} = C_{pvac} = -1.0$ signifies vacuum and $C_{plim} = C_{pcrit}$ implies $M_n = 1.0$ i.e. sonic flow.

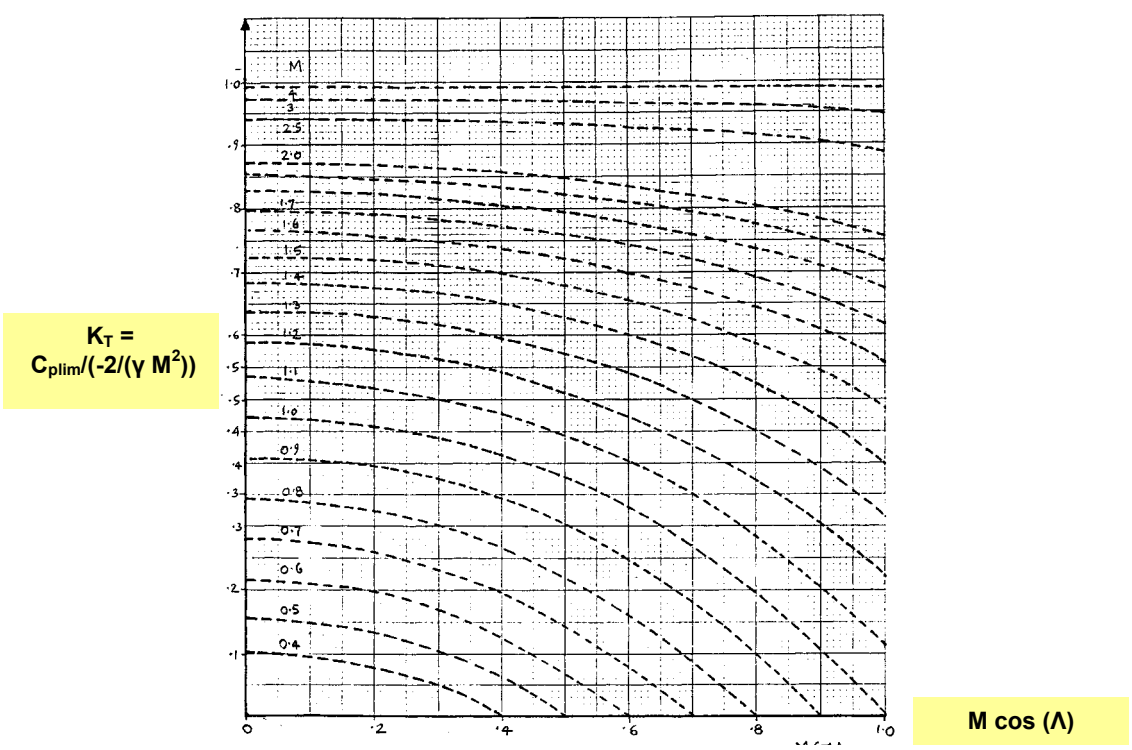

Figure 33-12: C_{plim} and Mach Number Relationships.

A typical C_p distribution for a symmetrical aerofoil section at a moderate AoA is illustrated in Figure 33-13. Integration of C_p values leads to local normal force coefficient C_{NL} and local thrust coefficient C_{TL} (c_n and c_t respectively in Carlson's notation). With AoA increasing, linear theory does not place any bounds on the magnitude of suction pressure, which therefore can become much greater than $-C_{pcrit}$ and any practically realizable value ($-C_{pvac}$). This can therefore severely limit the attainment of real thrust forces and adversely affect the prediction of aerodynamic properties, e.g. onset of flow separation, drag, lift and pitching moment.

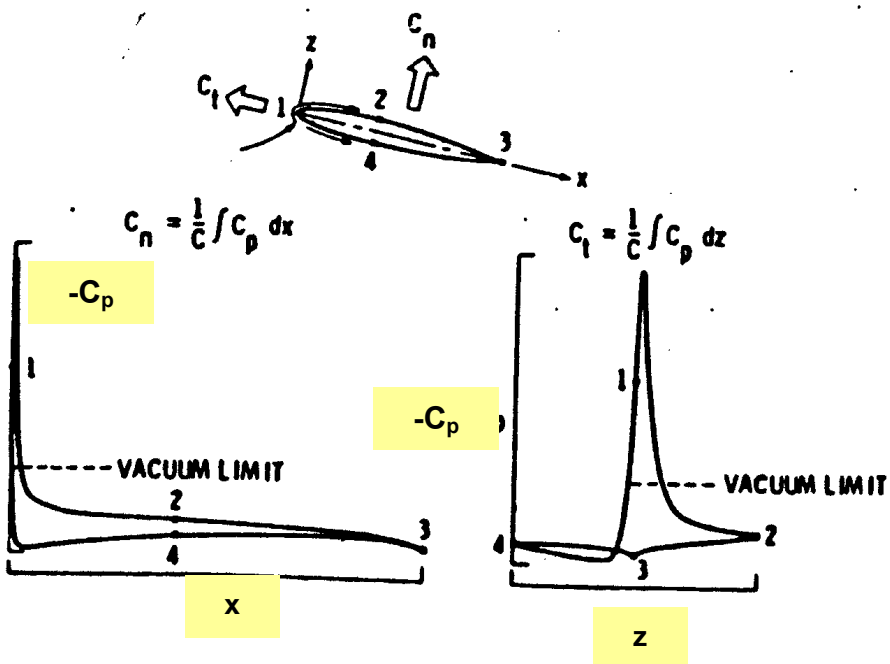

Figure 33-13: Typical Theoretical C_p Distributions and Local Force Coefficients c_t and c_n (Carlson).

The crux of the attained suction approach is to see how C_{plim} varies with suction level predicted on the basis of linear theory, flow parameters (Mach and Reynolds number) and geometry parameters of the aerofoil (r/c, t/c and position of maximum thickness x_m/c). The three-dimensional effects can be inserted via sweep theory. A Polhamus type approach allows the unattained part of the suction to be resolved into a non-linear force.

The prediction method needs, as a core, the attached flow properties (linear part) to develop the non-linear properties by adapting Polhamus LE suction analogy.

As mentioned in Section 33.3.2, for a sharp LE "uncambered" thin wing, all of the LE suction force is essentially "unattained" and this is "rotated" upwards giving rise to non-linear lift. This behaviour begins at 0° AoA.

Now, if the leading edge is not sharp then the flow "hangs on" and flow separation onset is delayed. The delay depends on:

1) The level of local LE suction;
2) The "local" aerofoil properties; and
3) The local Reynolds / Mach number combination.

This then becomes a function of y/s and helps in tracking the onset of flow separation and its development. On an aft swept wing with rounded LE, the flow separation begins from the wing tip area and travels inboard as AoA increases.

For an uncambered wing, at a given AoA, a rounded LE wing will have less total lift (linear + nonlinear) than that for a sharp LE wing.

In Carlson's approach, a series of 2-D aerofoils, Figure 33-14, were used to evaluate the 2-D limitations. The aerofoil thickness parameter (t/c) varied from 0.06 to 0.18. The aerofoil radius parameter (r/c) varied from 0.0012 to 0.0288. Maximum thickness of the aerofoil family was located at mid-chord.

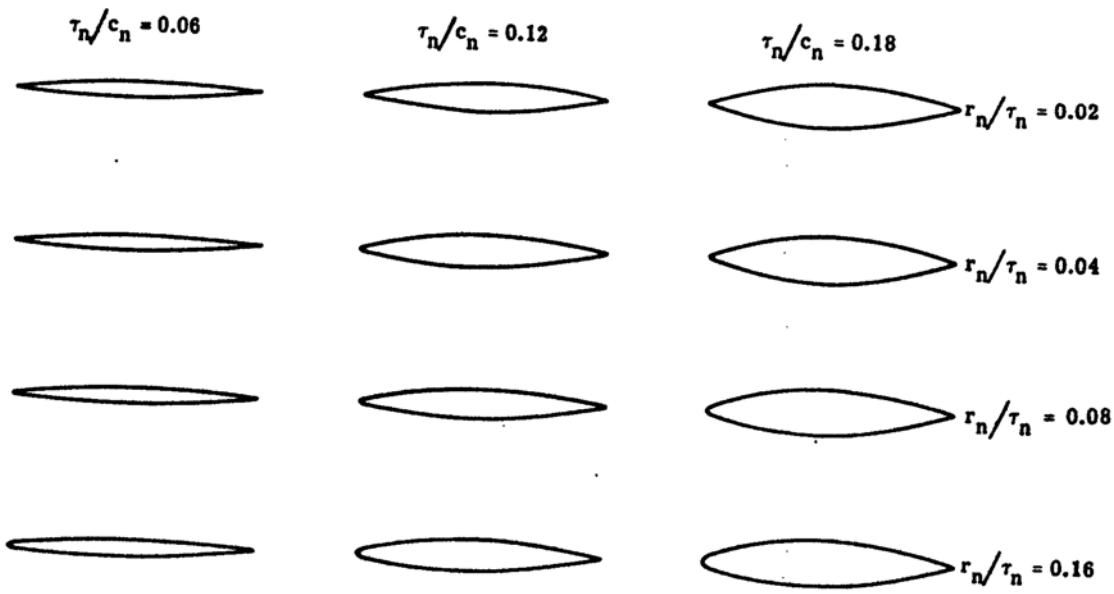

Figure 33-14: Family of Aerofoil Sections, Differing t/c, Maximum Thickness t_{max} at Mid-Chord (Carlson).

As the AoA increases or the Mach number increases, the magnitude of C_p reaches C_{pcrit} and then goes beyond C_{plim}, Figure 33-15. This allows the determination of factor K_T relating thrust with (given M) and without the vacuum limit (M = 0).

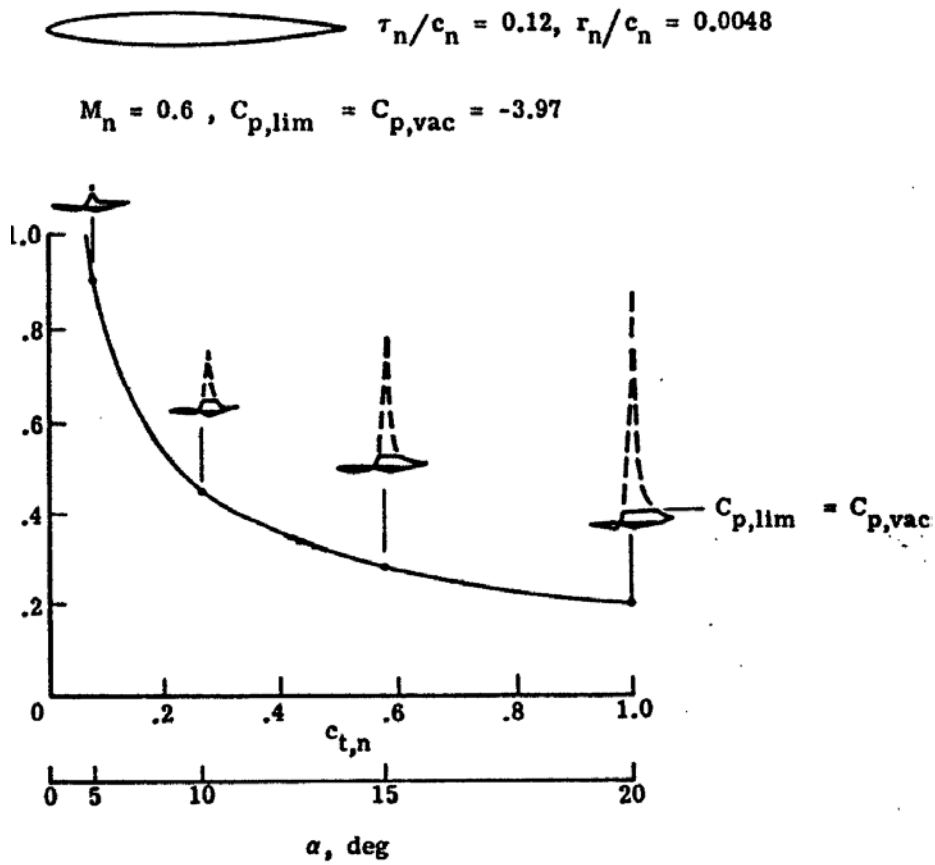

Figure 33-15: An Example of K_T Variation for AoA Increasing, Vacuum Limit (Carlson).

33.3.2.1 Mach and Reynolds Number Effects on C_{plim} or K_T

The values of C_{plim} and K_T are also subject to Reynolds number effects within two boundaries of:

1) K_T approaching 1.0 as Reynolds number approaches infinity; and
2) K_T will tend to vanish as Reynolds number approaches zero.

On the basis of experimental evidence, C_{plim} has been determined by Carlson et al, as a function of flow parameters normal to the leading edge: Mach number, M_n , and Reynolds number, R_n , see Figure 33-16. Figure 33-17 and Figure 33-18 illustrate two different curve fitted forms with parameter e_m (either 0 or an alternative value as in Figure 33-17).

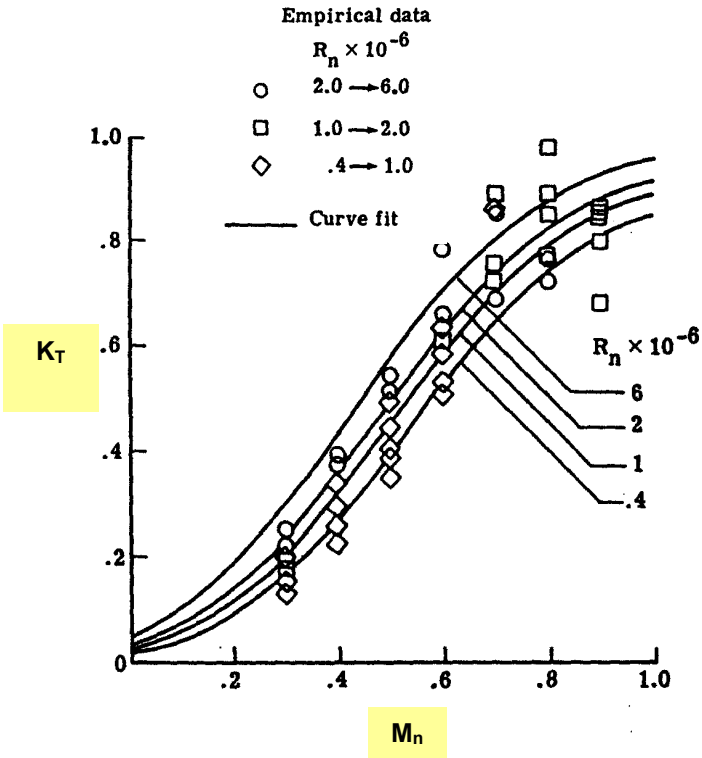

Figure 33-16: Dependence of K_T on Normal Mach Number and Normal Reynolds Number, Experiment and Theory (e_m = 0, see Figure 33-17) (Carlson).

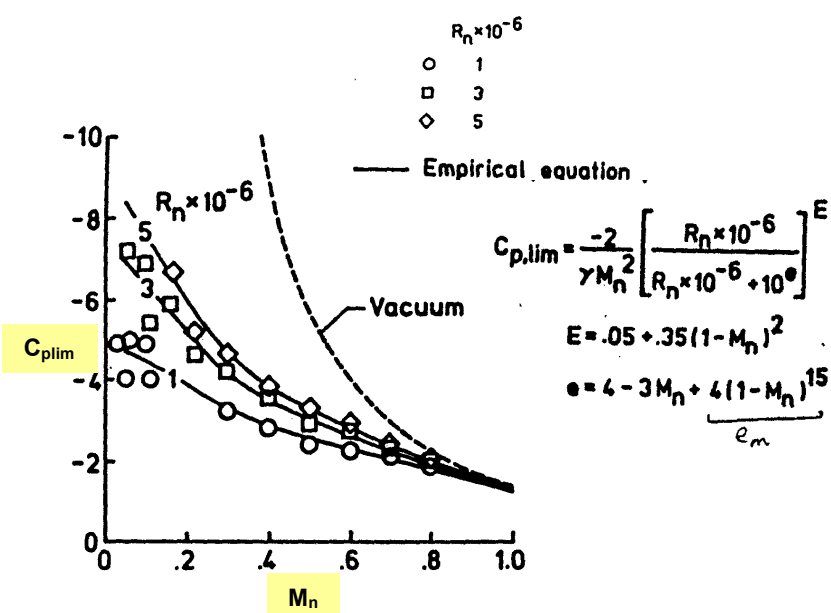

Figure 33-17: C_{plim} Variation with Normal Mach and Normal Reynolds Number, Experiment and Theory (e_m Finite as Defined) (Carlson).

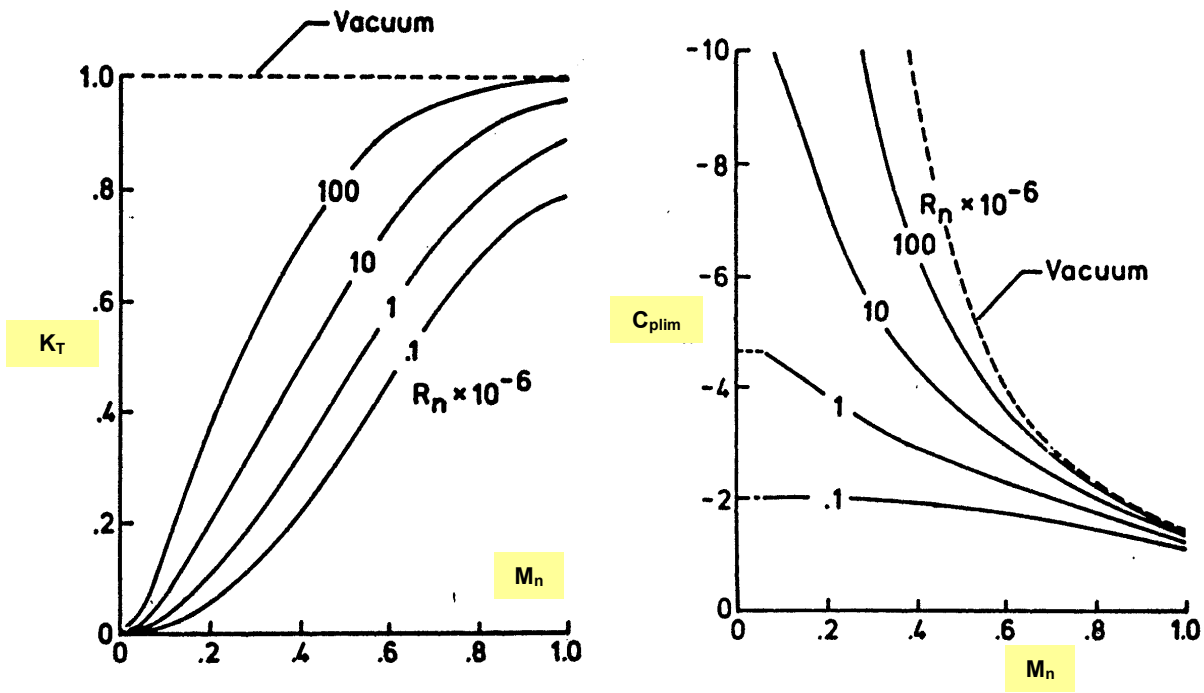

Figure 33-18: Variation of K_T and C_{plim} as Given by Carlson's Formula (e_m Finite as in Figure 33-17).

C_{plim} is also likely to be affected by the 3-D nature of the flow. For example, spanwise flow on the upper surface of a swept wing may relieve the adverse pressure gradient on certain areas (root of an aft-swept wing and the tip of a forward-swept wing). This can lead to achieving a higher C_{plim} over such areas.

General experience using Carlson's expressions incorporated into a vortex lattice lifting surface theory is that C_{plim} is under-estimated at the lower Mach numbers.

This led to further consideration by Nangia of available data for the extraction of C_{plim}. As a result, possible updates were produced for C_{plim} for R_n between 10^5 and 10^{10}. Figure 33-19-Figure 33-21 show the updates.

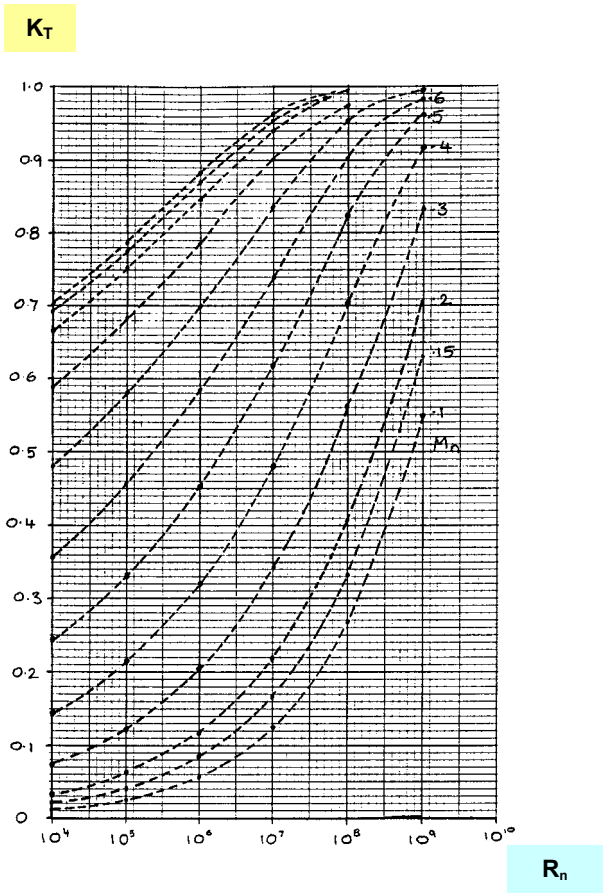

Figure 33-19: Variation of K_T with R_n, $e_m = 0$ (Carlson).

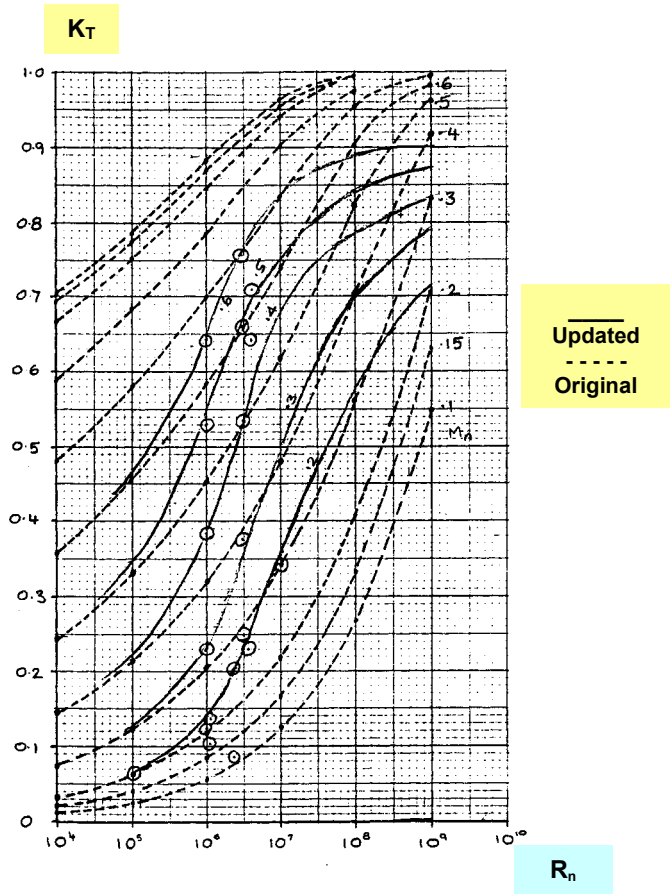

Figure 33-20: Updated Variation of K_T, R_n Varies between 10^4 and 10^{10}.

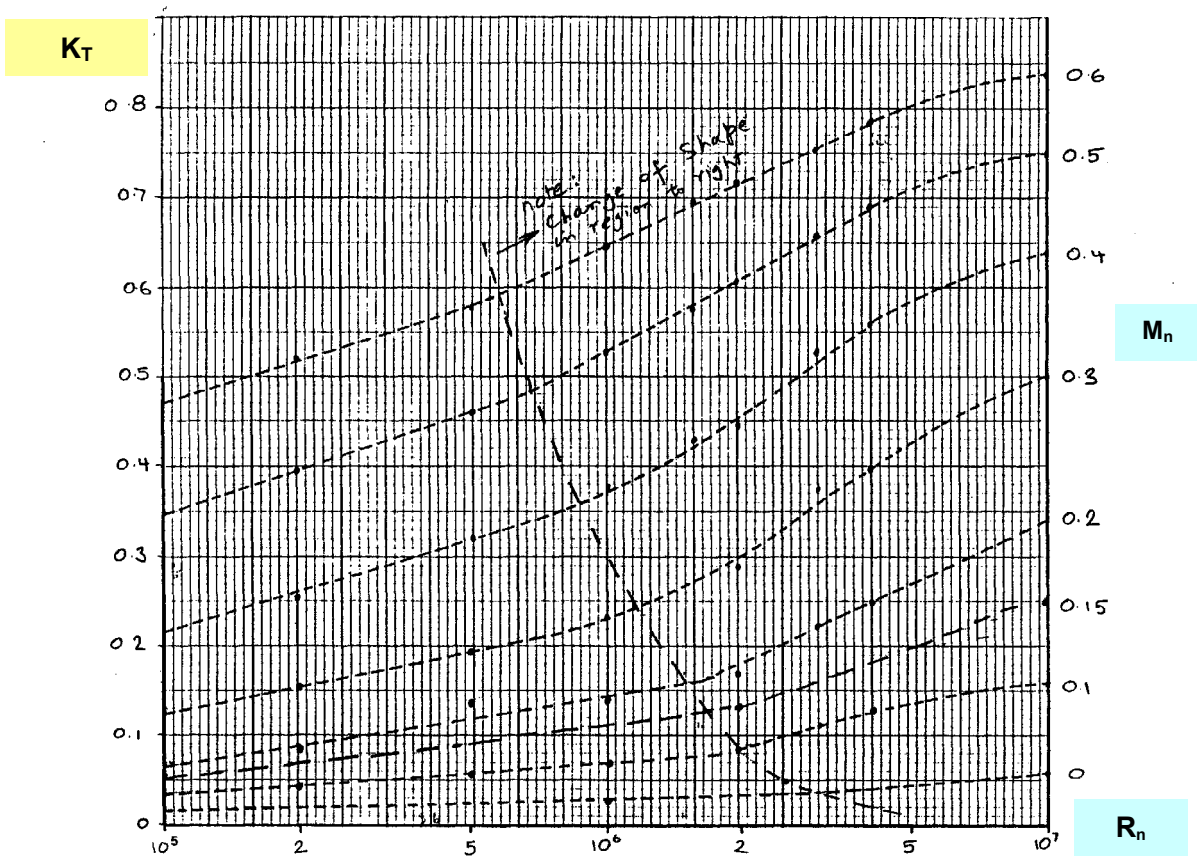

Figure 33-21: More Detail of Updated Variation of K_T, R_n Varies between 10^5 and 10^7.

33.3.2.2 Aerofoil Geometry Effects on C_{plim} and K_T

Following Carlson, K_T can be related to the aerofoil parameters as shown in Figure 33-22. The definition of normal aerofoil parameters (subscript n) follows from Figure 33-23 focussing on 3-D sweep relationships for a given planform.

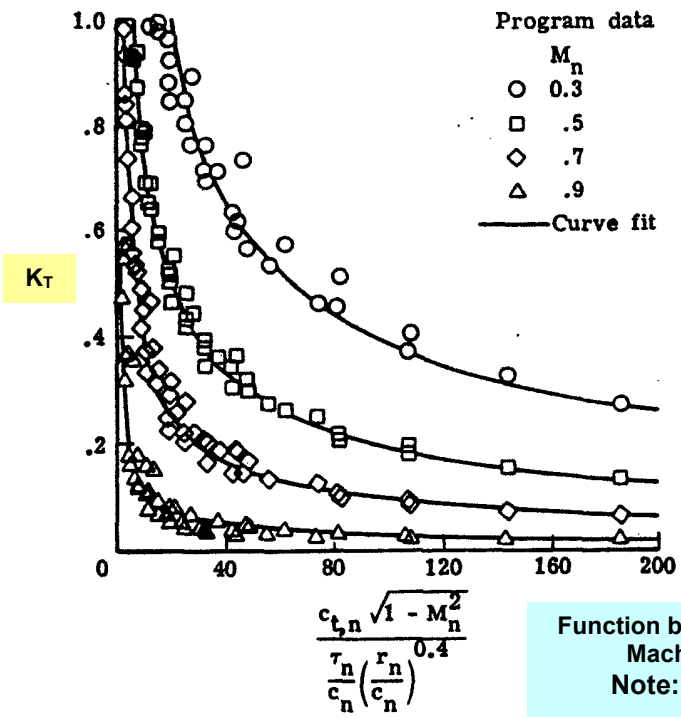

Function based on aerofoil geometry parameters, Mach number and Thrust parameters.
Note: $c_{t,n}$ is same as CTL, $\tau_n/c_n = t_n/c_n$

Figure 33-22: Dependence of Thrust Factor K_T on Normal Aerofoil Parameters and Normal Mach Number (see also Figure 33-23).

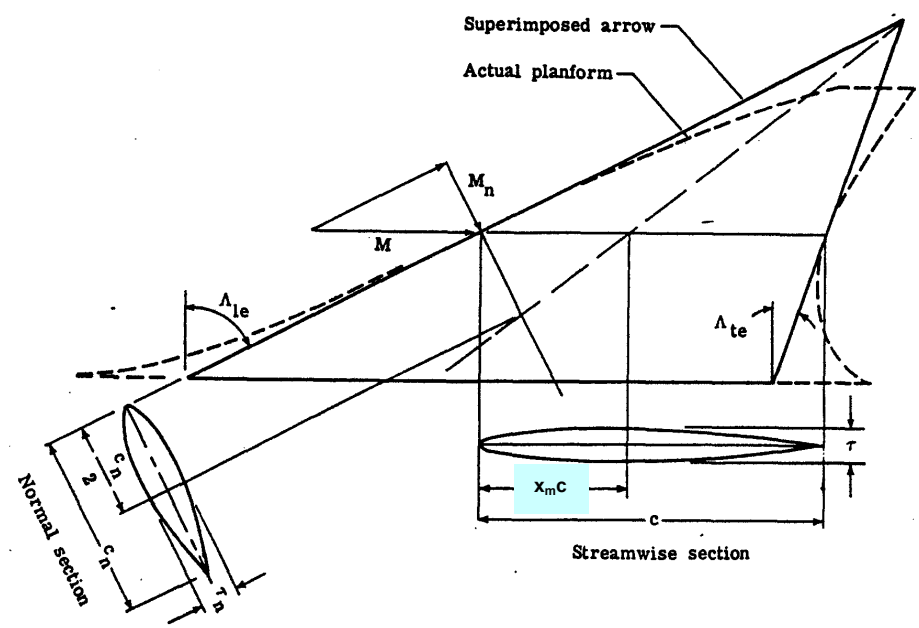

Figure 33-23: Sweep Theory and Definition of Normal Aerofoil Sections from Streamwise Sections of 3-D Wings.

33.3.3 LE Thrust Considerations for Swept 3-D Wings

The main steps are:

- The 2-D Considerations according to Section 33.3.2 are applied in the normal direction (n) of a swept wing (sheared wing part), Figure 33-23.
- The unusual 2-D cross-sections with flat upper and lower surface are transformed into "effective" aerofoils (normal to the LE) with assumed position of half chord.
- The ideal maximum C_{TL} distribution is modified for the root region and the tip region of the 3-D wing according to Kuchemann (Figure 33-24-Figure 33-27), resulting in a factor P_L (y/s), Figure 33-28.

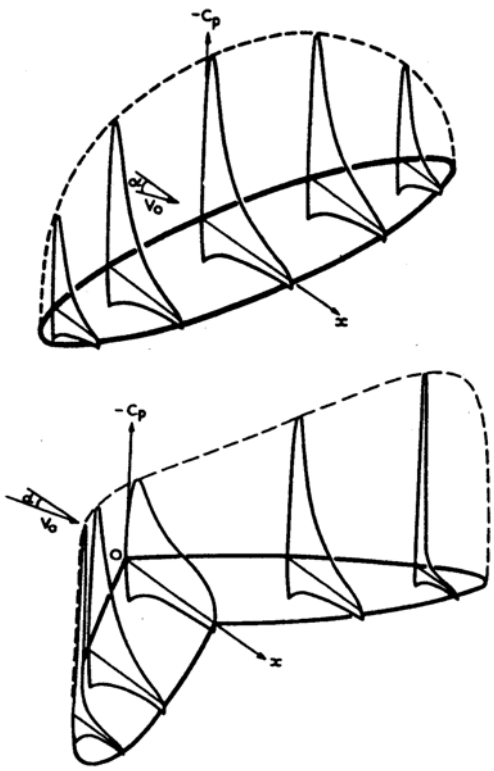

Figure 33-24: Pressure Distributions over Unswept and Swept Wings (Kuchemann).

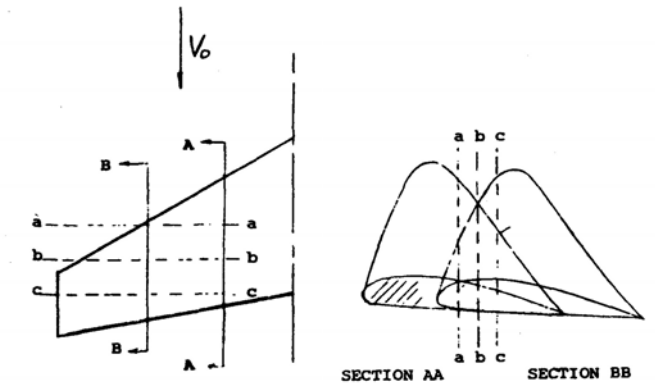

Section pressure distribution for swept back wings as influencing boundary layer flow.

Figure 33-25: Spanwise Flow and Alleviation of Gradients on Aft-Swept Wings.

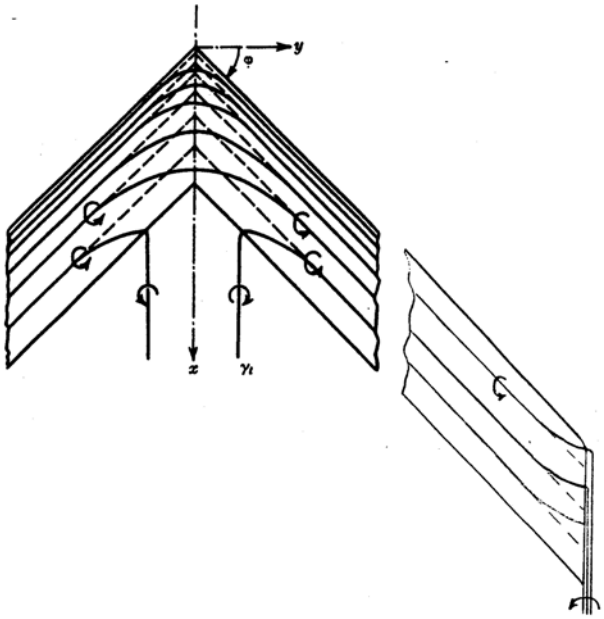

Figure 33-26: Vortex Lines Near the Centre and Tip of a Plane Swept Wing.

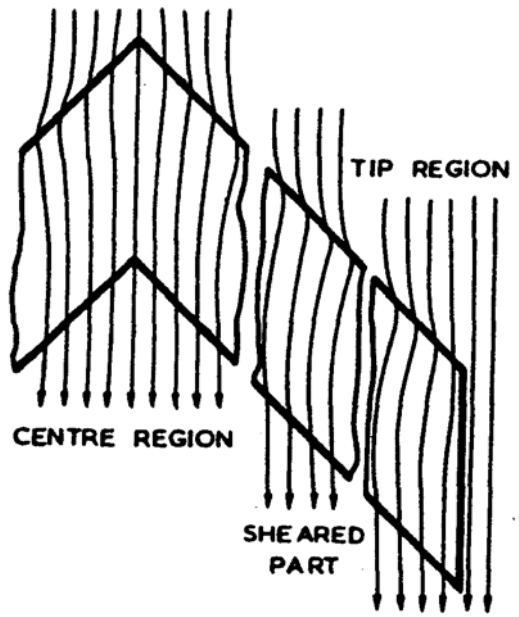

Figure 33-27: Streamlines Straightening at Wing Root and at Tip.

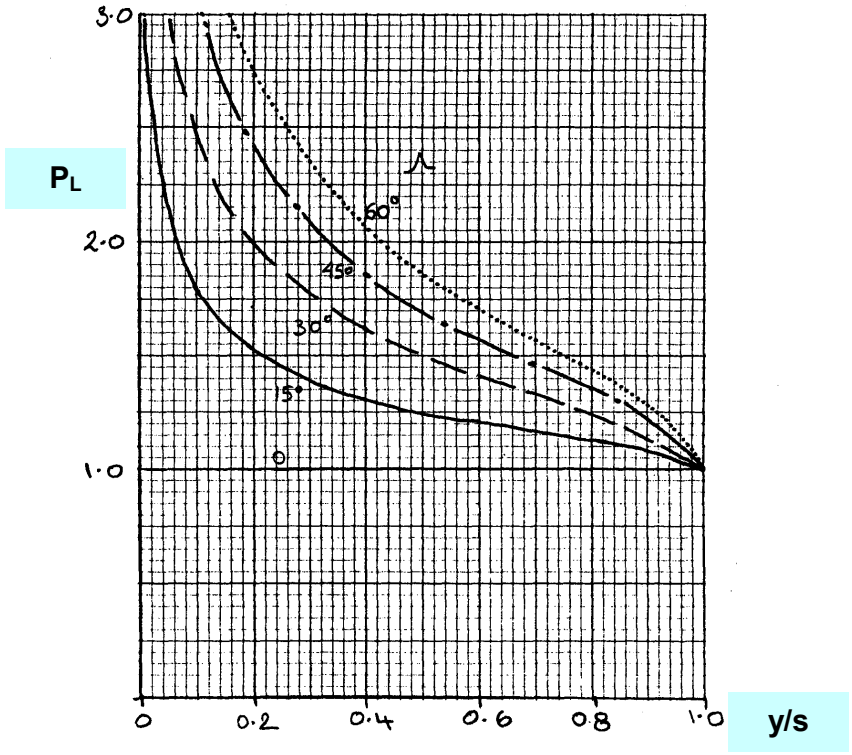

Figure 33-28: Typical Variation of P_L.

33.3.3.1 C_{plim} on 3-D Wings

This feature was neglected by Carlson. On a 3-D wing, C_{plim} near the leading edge of a swept wing is subject to boundary layer and varying pressure gradients along the wing-span, Figure 33-23. This may in some cases alleviate adverse interaction effects and thus imply higher C_{plim} values being attained over certain areas of the wing. In essence, the boundary layer flow acts in a manner similar to the use of suction for preventing separation and allows the wing section to develop a higher local lift coefficient than would be measured in 2-D flow. As shown in Figure 33-25 (based on Kuchemann, [33-16]), spanwise and chordwise pressure gradients interact as a result of wing sweep. Consider, on a swept-back wing, two chordwise pressure distributions (spanwise stations AA and BB) and y-z plane cuts at streamwise locations a, b and c. From a to b to c along AA, negative pressure (suction) tends to return to the freestream value. From a to b to c along BB, suction increases. Between a and b on AA the pressure remains more negative than between a and b on BB. There is no spanwise pressure differential between AA and BB at b. Between b and c on BB the suction increases whereas between b and c on AA suction decreases in magnitude. This mechanism causes the flow to move in the spanwise direction. Further, in the absence of a fuselage, the boundary layer is thinner near the wing root than at the wing tip of an aft-swept wing.

Kuchemann and others have shown that on swept-back wings, Figure 33-24 and Figure 33-26, the LE singularity strength and pressure gradients at the wing root are weaker than those at the mid semi-span of the wing. Near the wing-tip, LE singularity strength and pressure gradients are stronger than those at the mid-semi-span of the wing. The behaviour is reversed for forward-swept wings.

The curved streamlines typical of sheared-wing flow can persist neither into the center of the wing nor up to the wing tip. As sketched in Figure 33-27, the streamlines are straightened out in both regions.

After a great deal of analysis on a series of wings (unpublished work), it was found convenient to incorporate 3-D planform effects on C_{plim} by introducing a factor P_L (y/s):

$$C_{plim}\ (3\text{-D}) = P_L\ (y/s) \times C_{plim}\ (2\text{-D}).$$

A typical variation of P_L (y/s) for swept-back wings is given in Figure 33-28. Alternative forms for P_L (y/s) can be devised and a few of these have been studied. The current computer programmes allow the choice of using factor P_L (y/s) as needed.

33.3.3.2 Modelling Delay in Flow Separation Onset Due to Model Thickness

In view of the models unusual thickness distribution especially near the wing-tip, we may also need to include an additional feature to simulate the AoA delay in flow separation onset. This would appear to be a function of compressibility, LE radius and, or (possibly) the thickness terms at the tip region. We do not yet have a sufficiently convincing technique to include this term. The simplest technique for the present types of wing is to add on this term as a function of compressibility and LE radius thickness term:

$$\Delta(\text{AoA}) = dt^\circ \times \sqrt{(1-M \times M)} \times (r/\bar{c})^2, \text{ where dt is a suitable constant}$$

This function could be stronger at lower Mach numbers. Alternative proposals in terms of t/c near the wing tip are possible. The main inference is that further analyses using higher order approaches and correlations need to be obtained throughout the Mach number range. Experiments on VFE-2 will help.

33.3.4 Summarising the Process for Determining the Position of the Onset of Vortical Flow

For a given configuration geometry, AoA, Mach number and Reynolds number:

- Perform a linear solution by a Vortex / doublet lattice method and determine C_{TLmax} (or c_{tmax} , Carlson) distribution, modified for root and tip region (Kuchemann).
- Determine the local K_T thrust factor for given values of C_{TLmax} , Mach number, Reynolds number, Aerofoil section parameters normal to LE from the universal diagram (Figure 33-22).
- Compare maximum LE thrust C_{TLmax} and attainable LE thrust C_{TL} (attained) = K_T x C_{TLmax} , as a function of spanwise dimension. We note that if $C_{TL} = C_{TLmax}$ then the flow is attached. For $C_{TL} < C_{TLmax}$, the flow is separated.
- As in Polhamus's work, any reduction in axial force is turned by 90° and added to the lift. This corresponds to non-linear lift.

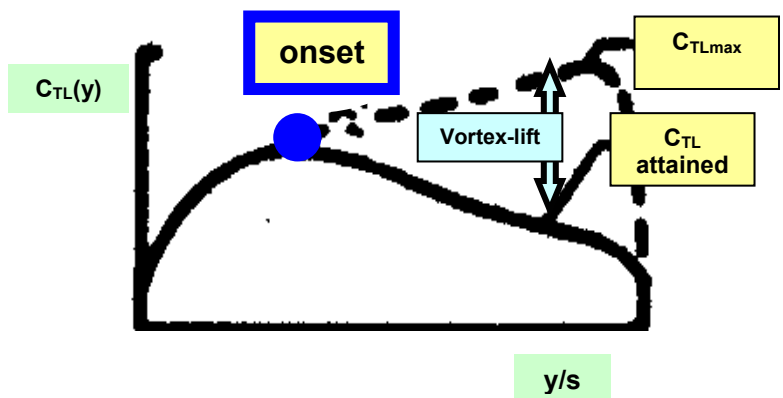

Figure 33-29: Determination of the Separation Onset.

33.3.5 Remarks

The application of the theory has a bearing on several issues e.g.:

- The unconventional aerofoils of the present delta wings might lead to improvements / modifications of the Carlson curve-fit formulae.
- The effects of Reynolds number on the $-C_{plim}$ reduction might also be different for the present unconventional aerofoils.
- Other inferences / criteria from the present approach to explain the differences for the large radius rounded LE configuration.

There are however issues such as non-standard aerofoil thickness distributions and Mach 0.85 application that need further understanding and verification. This can be enhanced by using higher-order solvers. In particular, an Euler solver could be used as a core solver along with the attained thrust approach. The thrust coefficient C_{TL} variations would then be based on the Euler results.

From a practical perspective, simple linear theory has limitations in modelling configuration associated details, e.g. fuselage, nacelles, etc. Such limitations could be handled more easily with an Euler method.

33.4 COMPARISONS WITH VFE-2 EXPERIMENTS

33.4.1 Modelling Detail from NASA LaRC Work Programme on 65° Delta

Figure 33-1-Figure 33-4 from Refs. [33-4]-[33-6], refer to the 65° delta wing model and the NTF wind tunnel facilities. Geometric details of the model are given together with tunnel operating ranges in terms of Mach and Reynolds number.

For application of the theoretical techniques, the salient particulars of the NASA model are:

Root chord of 2.1445 ft, aerodynamic chord, $\bar{c}_r$ = 1.4297 ft, Wing Area S = 2.1445 ft^2, AR = 1.8652.

In the NTF, independent Mach and Reynolds number sweeps/variations were carried out at Mach 0.4, 0.6 and 0.85. Reynolds number R_{mac}, varied between 6 & 60 million based on the mean aerodynamic chord $\bar{c}$ of the delta.

Four representative Leading Edges with different LE radii (sharp, small, medium and large) were used by Luckring, Figure 33-5. The corresponding LE radius distributions varied from sharp to smooth.

Model & LE	$r_{le}/\bar{c}$	$t/\bar{c}$
Config. with sharp LE	0.0	0.051
Config. with small round LE	0.0005	0.051
Config. with medium round LE	0.0015	0.051
Config. with large round LE	0.0030	0.051

Essentially, all the models featured non-standard aerofoils because of large flat areas, joined with strongly curved LE and TE regions. Figure 33-4 showed the effective t/c and r/c distributions along the semi-span. Both these quantities are extremely large towards the wing-tip even with the small round LE. In most practical highly swept-back wing configurations, the bounds of t/c and r/c values are much lower. For example, supersonic configurations usually have t/c of the order of 2.5 to 3.5% along the span.

It also follows that t/s (s is local semi-span at a given x) is very large in the apex region. The edge angle is correspondingly fairly large and the sharpness of the LE may not dominate the characteristic flow in the apex region.

This poses special problems for assessments using simpler theory as some of the implicit empiricisms do not encompass very large local t/c, t/s and r/c values. Also most of the theoretical assumptions imply “standard” aerofoil shapes.

33.4.2 Results from Luckring’s Papers on Vortex Flow Onset (Figure 33-5 – Figure 33-8 of Section 33.2)

As mentioned in Section 33.2, for the different wings, Luckring presented a series of parametric results for the onset of flow separation (LE vortex) in Figure 33-5 – Figure 33-8. Mach and Reynolds number have been varied. It is useful to provide some further detail here. This is also further discussed in a separate Chapter.

For models with different rounded LE, Figure 33-5 shows the effect of R_{mac} = 6 & 60 million, on flow separation (LE vortex) onset and movement with respect to AoA. Note that the rounded edge delays the vortex onset. Onset occurs at higher AoA as Reynolds number increases.

For the model with medium rounded LE, Figure 33-6 shows the effect of compressibility (M = 0.4, 0.6 & 0.85) at Reynolds number (R_{mac} = 6 million) on flow separation (LE vortex) onset and movement with respect to AoA. Note that decreasing Mach number delays vortex onset. As Reynolds number increases, onset occurs at higher AoA.

For models with different rounded LE, Figure 33-7 shows the effect of compressibility (M = 0.4, 0.6 & 0.85) at Reynolds number R_{mac} = 6 million, on flow separation (LE vortex) onset and movement with respect to AoA. Note that the decreasing Mach number delays vortex onset. The delays are higher with roundness increasing. For the small LE roundness, there appears to be very little effect due to compressibility.

For the model with medium rounded LE, Figure 33-8 summarises the effect of compressibility (M = 0.4, 0.6 & 0.85) at R_{mac} = 6 & 60 million. This confirms the general inference that increasing Mach number promotes flow separation and increasing Reynolds number delays the separations.

33.4.3 Results and Comparisons

Using the current theoretical approach, we have predictions for the onset of vortical flow (wing-tip) on the various models and these have been compared with results available from Luckring's experiments.

Figure 33-30 refers to the Reynolds number R_{mac} = 6 million case, as a function of compressibility (Mach 0.4, 0.65 & 0.8) for models with different roundness. Theory and experiment results are shown separately prior to super-imposition. Note that agreement is very good at all Mach numbers for the small roundness wings. As roundness increases, the correlation is still within about 2° AoA at lower Mach numbers. The correlation improves as Mach number increases.

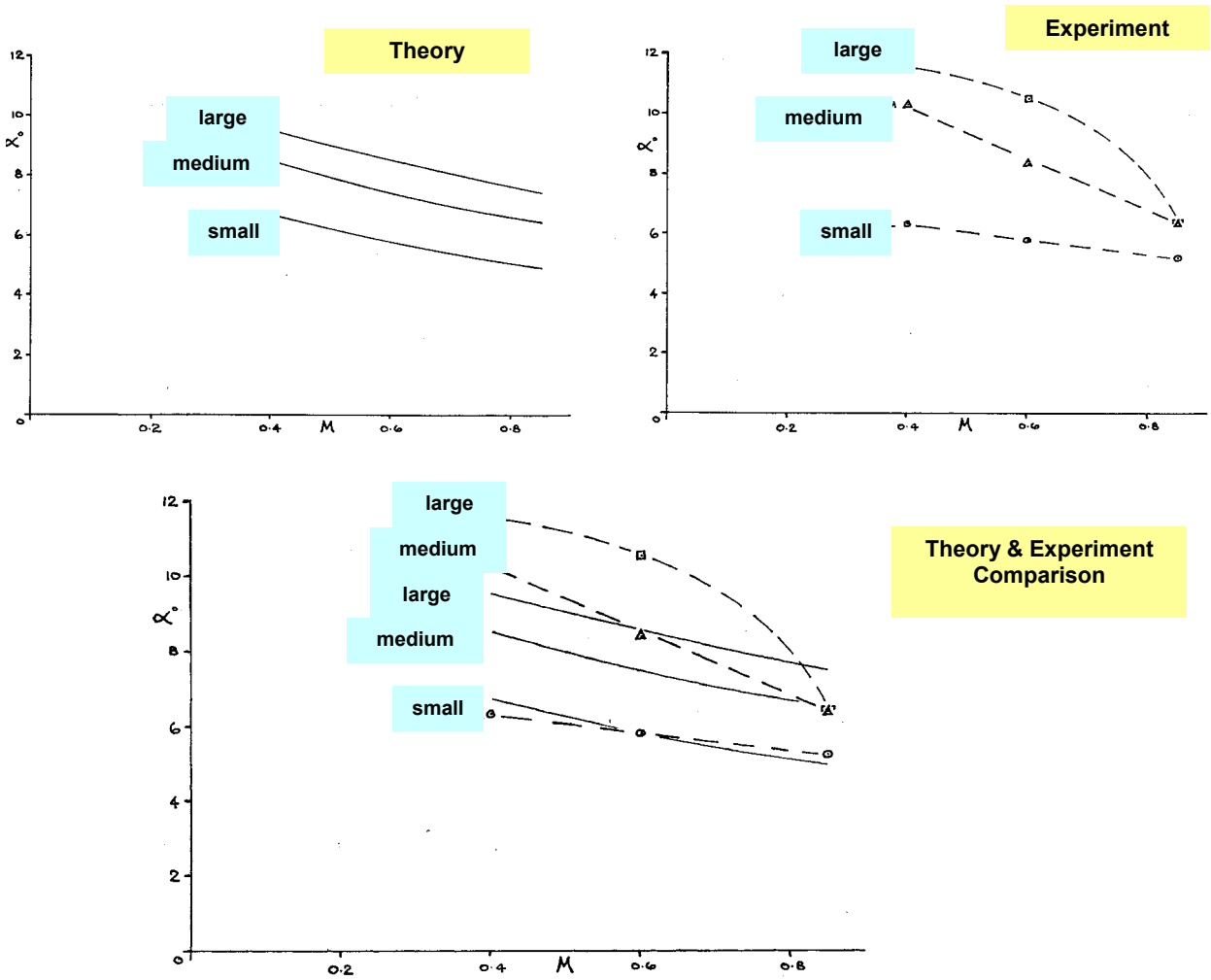

Figure 33-30: Onset of Separation at Wing-Tip, Theory and Expt. Small, Medium and Large Roundness Models, R_{mac} = 6 Million.

The results also suggest that there is a need for a delay term of the order of 2° – 3° for the higher roundness wings. It may be that vortical flow over the blunt edges arises inboard of the actual geometrical LE. This will then depart from the assumptions implied in the predictive approach.

For the small roundness model at Reynolds number R_{mac} = 6 million, Figure 33-31 shows the development of the onset of separation along the span (y/s scale) for Mach 0.4, 0.65 and 0.85. Note that y/s = 1.0 corresponds to x/c_r of 1.0. The agreement between theory and experiment is excellent over the wing span.

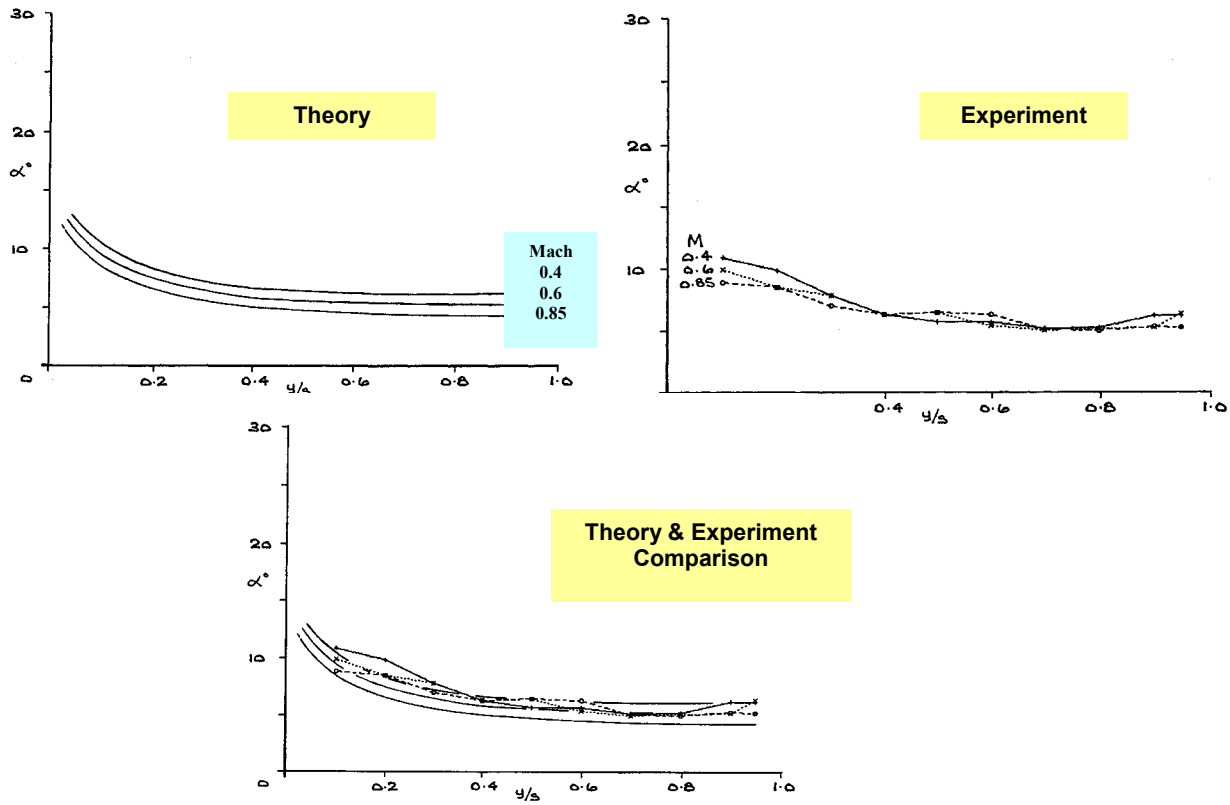

Figure 33-31: Development of Onset of Separation along Wing, Theory and Experiment, Small Roundness Model, R_{mac} = 6 Million, Mach Varies.

For the medium roundness model at Reynolds number R_{mac} = 6 million, Figure 33-32 refers to the development of the onset of separation along the span. Mach number values are: 0.4, 0.65 and 0.85. The agreement between theory and experiment is excellent at Mach 0.85. At Mach 0.6, the correlation is between about 1° AoA at the tip to about 2° in AoA at 0.2 y/s. At Mach 0.4, the correlation is between about 2° AoA at the tip to about 3° in AoA at 0.2 y/s.

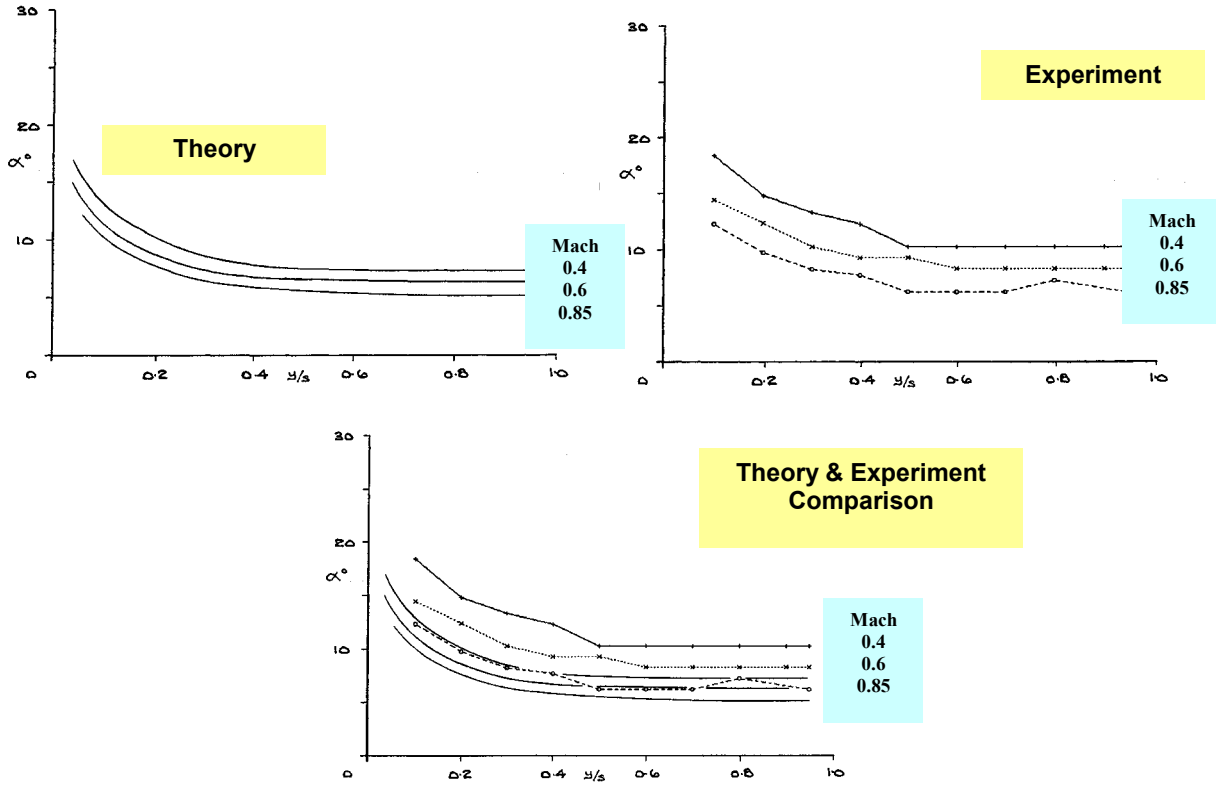

Figure 33-32: Development of Onset of Separation along Wing, Theory and Experiment, Medium Roundness, R_{mac} = 6 Million, Mach Varies.

For the large roundness model at Reynolds number R_{mac} = 6 million, Figure 33-33 refers to the development of the onset of separation along the span. Mach number values are: 0.4, 0.65 and 0.85. The agreement between theory and experiment is excellent at Mach 0.85. At Mach 0.6, the correlation is between about 3° AoA at the tip to about 5° in AoA at 0.2 y/s. At Mach 0.4, the correlation is between about 4° AoA at the tip to about 8° in AoA at 0.2 y/s.

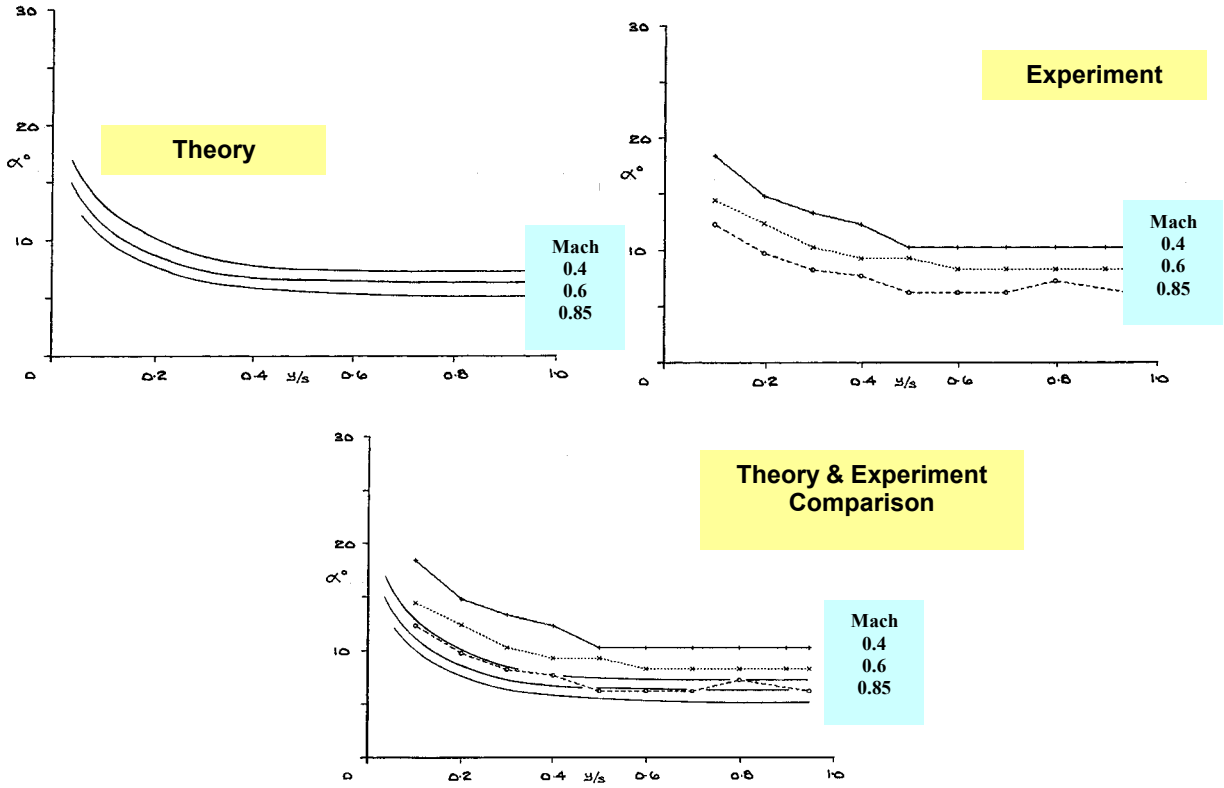

Figure 33-33: Development of Onset of Separation along Wing, Theory and Experiment, Large Roundness, R_{mac} = 6 Million, Mach Varies.

For Reynolds number R_{mac} = 6 million and Mach 0.4, Figure 33-34 refers to the development of the onset of separation along the span of the models with different rounded LE. For the small radius model, the agreement between theory and experiment is excellent over the whole span.

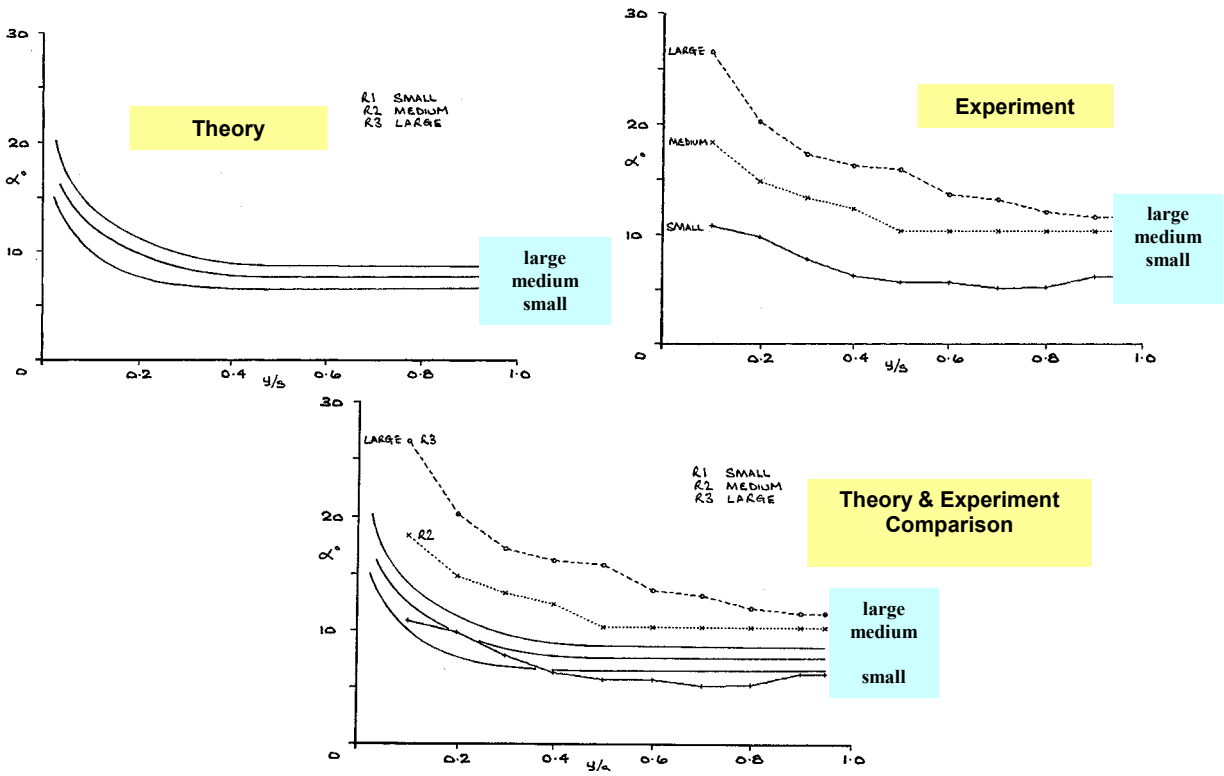

Figure 33-34: Development of Onset of Separation along Wing, Theory, Mach 0.4, R_{mac} = 6 Million, Small, Medium and Large Roundness Models.

For Reynolds number R_{mac} = 60 million and Mach 0.4, Figure 33-35 refers to the development of the onset of separation along the span of the models with different roundness. For the small radius model, the agreement between theory and experiment is excellent over the whole span.

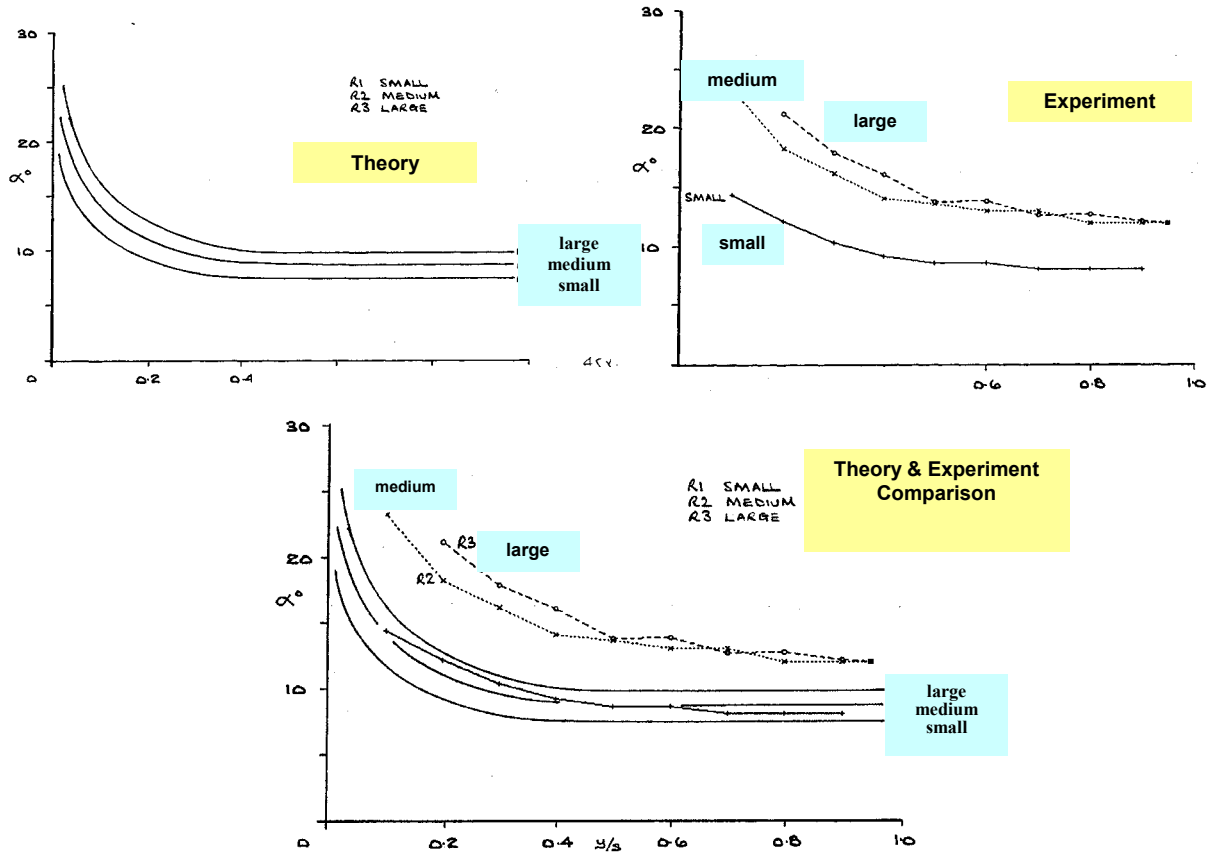

Figure 33-35: Development of Onset of Separation along Wing, Theory, Mach 0.4, R_{mac} = 60 Million, Small, Medium and Large Roundness Models.

33.5 CONCLUDING REMARKS

This paper is motivated via the initiative of the RTO-AVT Task group AVT-113. This task group has followed on from the previous AVT-080 group. One of the tasks, VFE-2, is concerned with theoretical and experimental activities on a series of 65° delta wings with different LE bluntness. These were initially tested by Luckring at NASA LaRC. This paper is concerned with the prediction of flow separation onset for VFE-2.

The models used by Luckring have been described. These featured somewhat unusual non-standard aerofoils and some of the local parameters and curvatures were very much larger than those expected on practical wings. Nevertheless useful experimental results for the onset of vortical flow were available with independent sweeps of Mach and Reynolds number (NTF-WT).

Details of the Attained suction approach have been given. It starts with a Subsonic lifting surface theory and incorporates Mach and Reynolds number and Attained thrust and Vortex Effects.

Results obtained for various wings have been compared with Luckring data. These show encouraging correlation for wings with small and medium radii. For the large radii LE, the correlations were “best” at the

higher Mach number. The large roundness model wing implies perhaps a different interpretation from the experimental data – separation may be appreciably inboard of the LE.

It must be remembered that we are predicting onset of flow separation. Vortex formation (as observed in experiments) could be delayed!

The challenge is there for developers to improve on the empiricisms. Further development can be envisaged on many aspects. Moderate sweep wings are of current interest e.g. on UCAVs.

The present work has allowed an understanding of the directions in which the empiricism can be improved e.g. using an Euler solver as the core solver.

33.6 ACKNOWLEDGEMENTS

This work is part of current in-house R & D activities. In early years (80s – 90s), some of the theoretical work was partly supported by the RAE (UK). The author has pleasure in acknowledging helpful discussions with Prof. D. Hummel, Dr. J.E. Lamar and Dr. J.M. Luckring. Thanks are due to Dr. M.E. Palmer for his patient technical assistance. Any opinions expressed are those of the author. The author has been privileged to be a member of AVT-113 Task Group. It is felt that the Task Group work has been truly inspirational and thorough, being accomplished by motivated and expert researchers. Opportunities for future collaboration are warmly invited.

33.7 REFERENCES

[33-1] Nangia, R.K. and Miller, A.S.: *Vortex Flow Dilemmas & Control on Wing Planforms for High Speeds*, RTO-AVT Symposium on "Advanced Flow Management, Vortex Flows & High Angle of Attack", Loen, Norway, May 2001, Meeting Proceedings RTO-MP-069 (I), SYA 9-1 to 9-14, 2003.

[33-2] AVT-080 Report. Published by RTO & Springer Verlag, 2007.

[33-3] Nangia, R.K.: *Applying Vortex Breakdown Empiricisms to Predict Aerodynamic Characteristics in Symmetric & Asymmetric Situations*, AIAA Paper 2003-3945, 2003.

[33-4] Luckring, J.M.: *Reynolds Number and Leading-Edge Bluntness Effects on a 65° Delta Wing*, AIAA Paper 2002-0419, 2002.

[33-5] Luckring, J.M.: *Transonic Reynolds Number and Leading-Edge Bluntness Effects on a 65° Delta Wing*, AIAA Paper 2003-0753, 2003.

[33-6] Luckring, J.M.: *Compressibility and Leading-Edge Bluntness Effects for a 65° Delta Wing*, AIAA Paper 2004-0765, 2004.

[33-7] Lamar, J.E.: *Some Recent Applications of the Suction Analogy to Vortex-Lift Estimates*, NASA-TM-X-72785, 1972.

[33-8] Lamar, J.E. and Campbell. J.F.: *Recent Studies at NASA Langley of Vortical Flows with Neighbouring Surfaces*, AGARD-CP-342, 10-1 to 10-27, 1983.

[33-9] Carlson, H.W. and Mack, R.J.: *Studies of Leading-Edge Thrust Phenomena*, J. Aircraft., Vol. 17, No. 12, pp. 890-897, 1980.

[33-10] Carlson, H.W., Shrout, B.L. and Darden, C.M.: *Wing Design with Attainable Leading-Edge Thrust Considerations*, J. Aircraft, Vol. 22, No. 3, pp. 244-248, 1985.

[33-11] Polhamus, E.C.: *Predictions of Vortex-Lift Characteristics by a Leading-Edge Suction Analogy*, J. Aircraft., Vol. 8, No. 4, pp. 193-199, 1971.

[33-12] Polhamus, E.C.: *Charts for Predicting the Subsonic Vortex-Lift Characteristics of Arrow, Delta, and Diamond Wings*, NASA TN-D-6243, April 1971.

[33-13] Lan, C.E. and Hsu, C.H.: *Effects of Vortex Breakdown on Longitudinal and Lateral Aerodynamics of Slender Wings by the Suction Analogy*, AIAA Paper 82-1385, 1982.

[33-14] Lan, C.E.: *Theoretical Prediction of Wing Rocking*, AGARD-CP-386, pp. 32-1 to 32-13, 1985.

[33-15] Tseng, J.B. and Lan, C.E.: *Calculation of Aerodynamic Characteristics of Airplane Configurations at High Angle of Attack*, NASA CR-4182, 1988.

[33-16] Kuchemann, D.: *The Aerodynamic Design of Aircraft*, Pergamon Press, Oxford, 1978.

[33-17] Nangia, R.K.: *The Design of Manoeuvrable Wings using Panel Methods, Attained Thrust & Euler Codes*, ICAS-92, China, 1992.

[33-18] Nangia, R.K. and Palmer, M.E.: *A Comparative Study of Four UCAV Wing Layouts – High-Speed Aero Performance & Stability Considerations*, ICAS – 2006-1.7, Germany, September 2006.